THE STRUCTURE OF THE OCEANIC CRUST ON THE NORTHEAST HAWAIIAN ARCH IMAGED BY PRE-STACK DEPTH MIGRATION OF ACTIVE-SOURCE SEISMIC DATA

A THESIS SUBMITTED TO THE GRADUATE DIVISION OF
THE UNIVERSITY OF HAWAI‘I AT MĀNOA
IN PARTIAL FULFILLMENT OF THE REQUIREMENTS FOR THE DEGREE OF

MASTER OF SCIENCE
IN
GEOLOGY AND GEOPHYSICS

MAY 2019

By
NIPAPORN NAKRONG

Thesis Committee:
Gregory F. Moore, Chairperson
Brian Taylor
Robert Dunn

Keywords: Mohorovičić Discontinuity, NE Hawaiian Arch, Pre-Stack Depth Migration, Lower Crustal Dipping Reflection, Sub-Moho Event, Oceanic Crustal Thickness

Acknowledgments

First, I would like to thank my thesis advisor Professor Gregory F. Moore of the Department of Earth Sciences (formerly known as the Department of Geology & Geophysics), the School of Ocean and Earth Science and Technology, at the University of Hawai‘i at Mānoa. Since the beginning of my degree, he always answered emails quickly, and kept of track of my thesis. When I ran into trouble, I could ask Prof. Moore for help.

I would also like to acknowledge Professor Brian Taylor and Professor Robert Dunn, two of my thesis committee members who provided valuable suggestions for my thesis.

I could not be here without the funding from my scholarship, the Development and Promotion of Science (DPST) and Technology Talents Projects, the Promotion of Teaching Science and Technology (IPST), and the Royal Thai Government. They have provided me a fully funded scholarship since high school until present. I received valuable and precious experience in study and unbreakable friendships during my participation in this program.

A thank you also goes out to all my friends who always encouraged me to not give up. Thank you for listening, offering me advice, proofreading my terrible writing and giving me lots of useful suggestion both in study and life.

In addition, a thank you to Masako Robb who taught me how to use the seismic program and suggested useful seismic processing steps to me.

I would like to thank Mikiya Yamashita for giving me suggestions for this project.

This thesis is the journey of M.S. which is one essential key to reach my career goal. Thank you for my dedication to finish this degree.

Finally, I must express my profound gratitude to two of my lovely aunts, Miss Kitrung Supapornoran and Miss Junlada Saetae, my father and my boyfriend for providing me continuous

encouragement throughout my years of study. I knew that I studied so long for several years and had not much time to spend with you. You understood what I was doing and believed in me. I would love to make you proud of me.

Abstract

The Northeast Hawaiian Arch off O‘ahu, formed by flexure of the Pacific Plate under the load of the Hawaiian volcanic island chain, is one of the regions under consideration for Integrated Ocean Drilling Program (IODP) drilling through the oceanic crust to the Mohorovičić discontinuity (Moho). Modern geophysical surveys in this area, including wide-angle seismic refraction data and multi-channel seismic reflection data (MCS), are insufficient for imaging the oceanic crustal structure and the Moho characteristics in order to define the potential drilling site. Therefore, the Japan Agency for Marine-Earth Science and Technology (JAMSTEC) carried out an active source 2-D seismic survey along the Hawaiian Arch using R/V *Kairei* in August and September 2017. One 750-km-long E-W reflection profile, shot perpendicular to abyssal hill (spreading) fabric, passes over five ocean bottom seismometers (OBS) with 150-km interval; three shorter N-S profiles were shot perpendicular to the long line at the OBS locations. We conducted pre-stack depth migration (PSDM) in an attempt to better image the Moho reflections than is possible with post-stack migration. The PSDM images confirm that the crustal thickness is approximately 5.4 km with a standard deviation of 0.3 km. Moho reflection is identified 50% of all lines, including shingled Moho (5%) and diffusive Moho (45%). Lower crustal dipping reflections (LCDRs) found at the east edge of Line E-W dip 5^{o} to 12^{o} toward the paleo-ridge axis and terminate at the Moho. These LCDRs may originate from a secondary shear zone due to active magma upwelling at the time of crustal accretion. We found the thick MTZs (>100m), imaged as the diffusive Moho, commonly accompanied by sub-Moho events.

Table of Contents

List of Tables

List of Figures

1. Introduction

The seismic velocity discontinuity located at the crust-mantle boundary zone is known as the Mohorovičić discontinuity (Moho). This refers to the increase in P-wave velocity to 7.6 - 8.6 km/s (Steinhart, 1967). In seismic imaging, the Moho is regularly a transition zone rather than a single discontinuity (Aghaei et al., 2014). The Moho transition zone (MTZ) indicates the separation of layered gabbro and residual peridotite and defines as the top of the upper mantle (Nedimovic et al., 2005). The typical thickness of oceanic crust ranges between 5 to 8 km below the seafloor (BSF) (Jarchow and Thompson, 1989) and generally depends on crustal age, accretionary processes at the mid-oceanic ridge and seafloor spreading rate (Mutter and Carton, 2013; Ohira et al., 2017). From two-ship Expanding Spreading Profile (ESP), the Moho depth at the Hawaiian Arch is approximately 6.3 km beneath the seafloor (Watts et al., 1985).

The effort of drilling into the earth's oceanic crust started in the 1960s. The first attempt penetrated to 183 meters BSF off the coast of Mexico. The second attempt was located off the coast of Costa Rica at Deep Sea Drilling Program (DSDP) Site 504B, drilling into the complex dike-gabbro transition at 1507m. Several additional DSDP, Ocean Drilling Program (ODP) and Integrated Ocean Drilling Program (IODP) expeditions have been carried out around the world with the aim of drilling deeper into the oceanic crust. A site on the NE Hawaiian Arch was proposed in order to demonstrate the details of fundamental process, physical and chemical properties in the lower crust and the uppermost mantle.

In the next decade by 2030, the Moho project on the NE Hawaiian Arch may be launched. The Japan Agency for Marine-Earth Science and Technology (JAMSTEC) plans to drill into the Earth's crust at the Hawaiian Arch, northeast of O'ahu, by using the D/V *Chikyu*, the advanced

deep see drilling vessel equipped with riser drilling technology. An active seismic experiment was carried out in order to obtain the necessary data, including the nature of the Moho reflection, variability of the thickness and velocity structure of the crust-mantle boundary, and to decide whether the NE Hawaiian Arch is suitable for scientific deep hole (MoHole) drilling.

The development of marine geophysical surveys gives us greater knowledge and better understanding of the Moho and the oceanic crustal structure. Multi-channel seismic reflection (MCS) data are efficiently used to visualize the internal structure of the upper part of the oceanic crust (Vuong et al., 2011). Our study area is at the NE Hawaiian Arch, ~200 km away from the O‘ahu Island. In our project, 2-D MCS and wide-angle Ocean Bottom Seismograph (OBS) data were acquired from R/V *Kairei* between September and October 2017 to analyze details of crustal thickness, to interpret the characteristics of the Moho and the local P-wave velocity (Vp) profiles and to identify intra-crustal reflections. We aim to determine oceanic crustal thickness and structure, especially in the lower crust and the upper mantle.

1.1 The geological setting

The 10,000-km-long spreading ridge between the Pacific and Farallon plates is called the Pacific-Farallon Ridge (PFR) (Rowan and Rowley, 2014). The PFR formed the oceanic crust with an equatorial spreading rate of 13.5 cm/year (Handschumacher, 2013) and produced approximately 45% of all oceanic crusts formed in the past 83 Ma (Rowan and Rowley 2014; Fig. 1). Most of the conjugate Farallon plate has been subducted beneath the North American plate (Rowan and Rowley, 2014). The oceanic crust, the Pacific plate, at the Hawaiian Arch was generated at the PFR approximately 80 Ma ago (Late Cretaceous period; Clague and Dalrymple, 1989; Kay, 1994) with 35-40-mm/year half spreading rate, north of Molokai Fracture Zone (Müller et al., 2008).

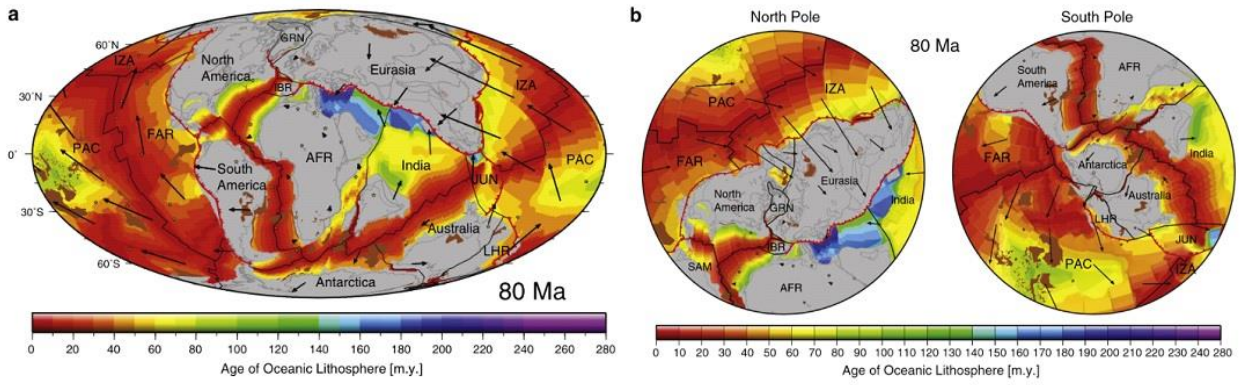

Figure 1 A 80 Ma global plate reconstruction (Seton et al., 2012). These maps, (a) and (b), illustrate the distribution of age and area of oceanic lithosphere at 80 Ma ago. Mid ocean ridges and transform faults are imaged by black lines. Products of plume-related excessive volcanism area indicated by brown polygons. PAC stands for the Pacific plate. FAR is Farallon. IZA is Izanagi. JUN is Junction. AFR is Africa. IBR is Iberia. SAM is South America. GRN is Greenland. LHR is Lord Howe Rise.

The Hawaiian Arch, a large arcuate flexural bulge due to the volcanic load by the Hawaiian hotspot chain, is 200 miles wide and more than 600 miles long. The average Moho depth over the Hawaiian Arch is approximately 10 km below sea level (BSL) (Furumoto and Woollard, 1965; Shor and Pollard, 1964) and can be as shallow as 9 km (Furumoto and Woollard, 1965). The Vp at the Moho over the arch, at section 28-30 (Fig. 2), changes from ~7 km to ~8 km/s. A multichannel seismic study carried out by two ships over the Hawaiian-Emperor Seamount chain demonstrates a deep crustal body ~ 4 km thick, with Vp of 7.4 to 7.8 km/s, assumed to be a deep crustal sill complex (Watts et al., 1985). It lies beneath the flexed oceanic crust. The Vp at the Moho of ESP 6 (Fig. 3), near our survey line, was estimated to change from 7.1 to 8.2 km/s. The Moho reflection is stronger south of the Hawaiian chain than to the north.

In the western section of Line E-W, the area is covered by the North Arch Volcanic Field (Fig. 5). It is a submarine alkalic series lava located on the Hawaiian Arch, NE of O‘ahu (Dixon et al. 1997; Davis and Clague 2006). The North Arch Volcanic Field related to the Hawaiian hotspot had started to erupt from ~1.15 Ma until ~0.5 Ma (Frey et al., 2000). The ~25000-km^2 volcanic lava flooded above the North Arch with tens-of-meters thickness (Clague et al. 2002;

Bianco et al. 2005). The eruption of the North Arch lavas on the plume track can affect the oceanic crustal structure and the Moho reflection. Therefore, our study can be used to demonstrate whether the North Arch Volcanic Field affects the structure of oceanic crust in our study area.

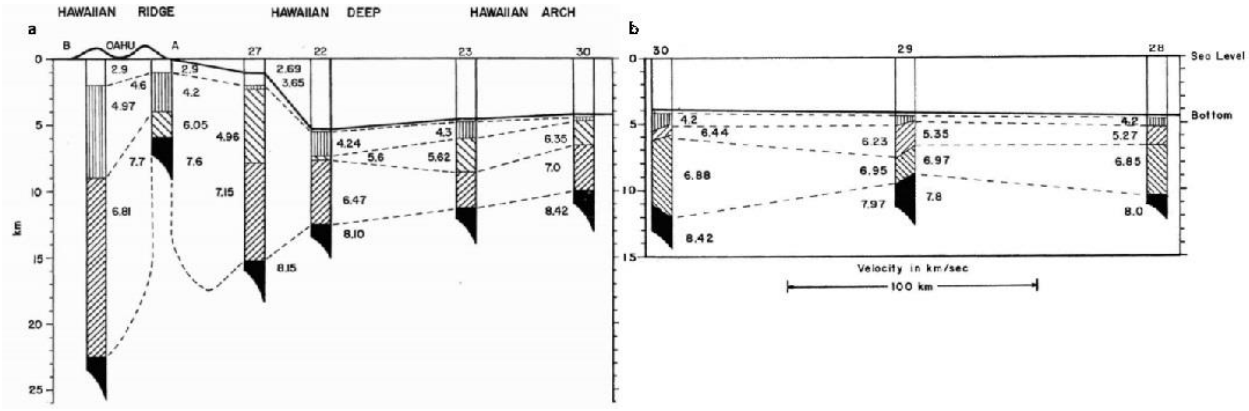

Figure 2 The Vp profiles between the Hawaiian Ridge and the Hawaiian Arch, (a), and across the Hawaiian Arch, (b), (Furumoto and Woollard, 1965; Furumoto et al. 1965; Shor and Pollard, 1964). The unit is in km/s.

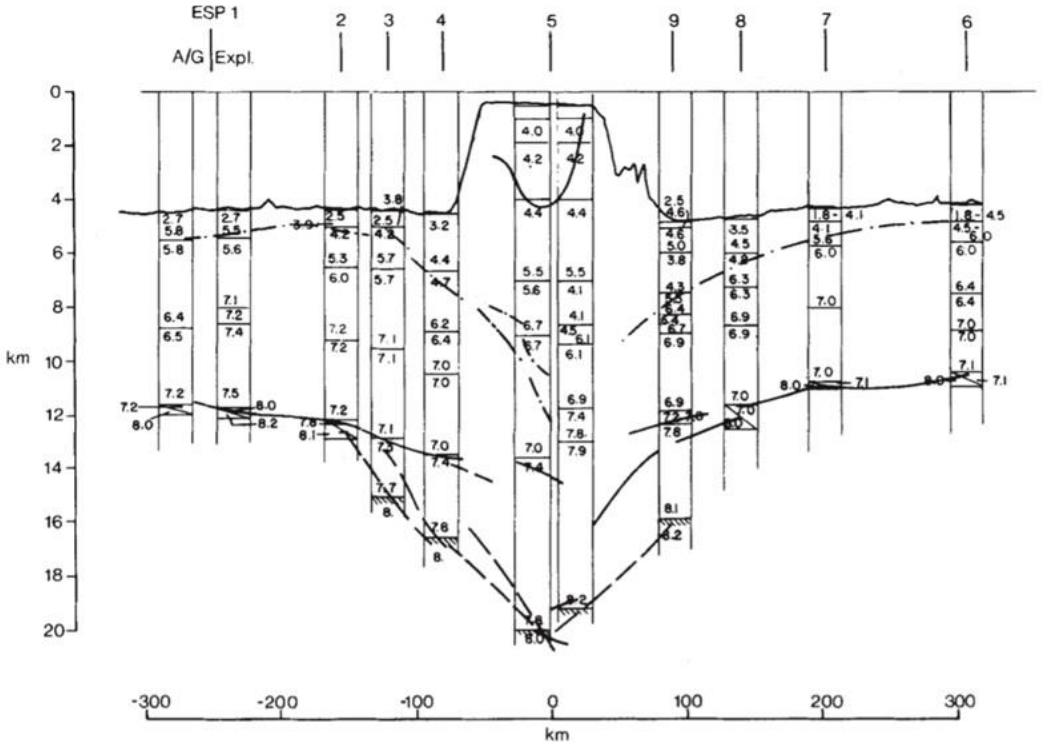

Figure 3 The Vp profile across the Hawaiian Island from south to north on ESPs 1 – 9 (Watts et al., 1985). The unit of numbers shown the prominent features in the oceanic lithosphere due to volcanic loading is in km/s. The location of ESP 6 is at the northern edge.

1.2 Objectives

1.2.1 To identify the Moho characteristics which is the seismic reflectors that separated the lower crust and the uppermost mantle.

The Moho characteristics in seismic images can be divided into three types; impulsive, shingled, and diffusive reflections (Kent et al. 1994; Aghaei et al. 2014; Fig. 4). Both the impulsive and shingled Moho reflections are single-phase events. Impulsive Moho reflections are continuous lines, while shingled Moho reflections have vertical offsets and can be overlapping. At the MTZ, if the Moho reflections can be identified as more than one reflection, or a multi-phase event, we indicate them to be diffusive Moho (Aghaei et al. 2014; Nedimović et al., 2005). It is associated with a thick Moho. The heterogeneity of crust-mantle interactions can generate these variations in characteristics of Moho (Aghaei et al. 2014). If the amplitude of Moho reflection is very weak but traceable, we interpret it to be weak Moho.

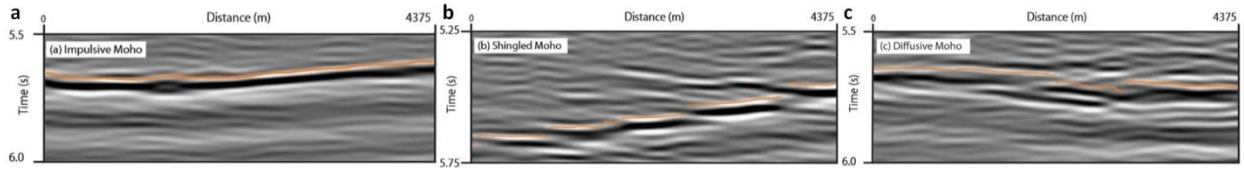

Figure 4 Post-Stack Time Migration of three types of Moho characteristics at the fast-spreading East Pacific Rise from 9º42'N to 9º57'N (Aghaei et al., 2014). (a), (b), (c) show the impulsive Moho, the shingled Moho, and the diffusive Moho, respectively.

1.2.2 *To image the oceanic crustal structure, especially between the lower crust and the upper mantle, by using Pre-Stack Depth Migration (PSDM) from MCS data*

PSDM was used to image seismic reflection profiles of 15 km BSL, including water column, oceanic crust, and upper mantle. Our focused depth is located from ~7 to 15 km BSL.

2. Data Acquisition

In 2017, five OBSs were deployed on the R/V *Marcus G. Langseth* and recovered on the R/V *Kilo Moana* after approximately twenty days along the NE Hawaiian Arch. The line of OBSs is roughly perpendicular to the age isochrons of the oceanic crust (Fig. 5). The distance between each OBS is 150 km. The nearest distance of an OBS to the Hawaiian Islands is ~200 km away from Oahu Island. This wide-angle seismic reflection/refraction survey lines were designed to image the deep lithospheric structure (Ohira et al., 2018).

The seismic survey was carried out using the R/V *Kairei*. A single MCS line (Line E-W) passes across the arch, some part of the North Arch Volcanic Field, and the back of the arch (Fig. 5). Three N-S MCS lines were shot over OBS1, OBS2 and OBS5, respectively, to acquire seismic reflection and wide-angle seismic refraction. In this project, we focus on the MCS data of the first ~350 km of Line E-W across the arch and two N-S lines, including Line N-S-1 and Line N-S-2 (Fig.5).

Table 1 Types of observation in our survey on R/V *Kairei*

List of observations	Observation instruments
Bathymetry	Multibeam sonar bathymetry mapping by SeaBeam 3012
Seismic Reflection	*Seismic source:* 4 sub-arrays (32 units) with 7800-cu.in total volume of tuned airgun array *Streamer:* 6-km long, 444 channels *Shot spacing:* 200 meters for OBS data and 50 meters for MCS data

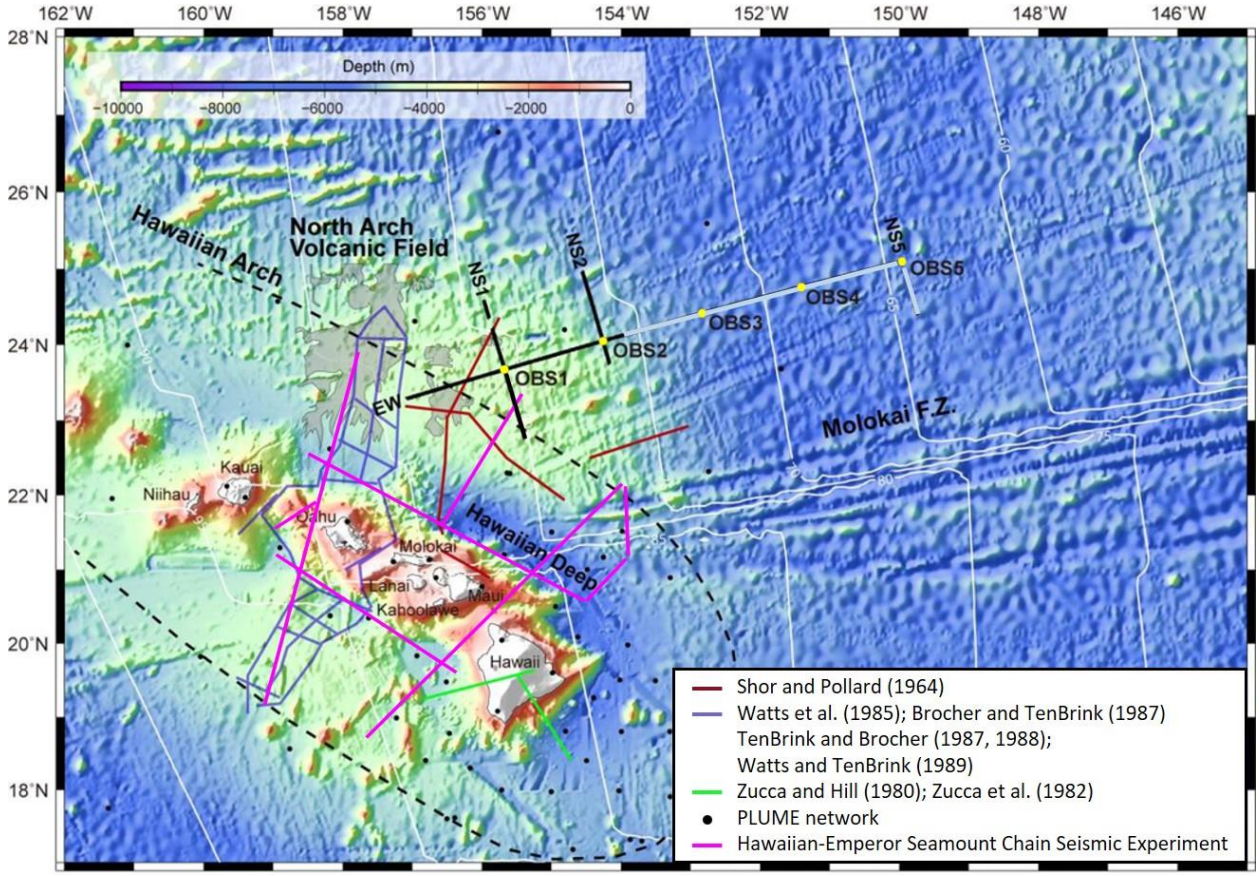

Figure 5 Bathymetry with crustal age contour of the Hawaiian Region (edited from Ohira et al., 2018). The age of oceanic crust in the seismic profiles ranges between 60 and 85 Ma. Ohira et al. (2018) interpreted the MCS profiles shown by the black and white lines. Our project is focused on the black line, where the crustal age ranges from 76 Ma in the east to 84 Ma in the west near the potential drilling site. The black dashed line is the axis of the Hawaiian Arch.

Table 2 The length of three seismic reflection profiles

Line	**EW**	**N-S-1**	**N-S-2**
Length (km)	355	213	140

3. Seismic reflection processing

The MCS lines were processed by a conventional seismic processing flow using Paradigm software. After resampling the data to 4 ms, band-pass filtering was applied to remove noise outside the range of 2-5-90-100 Hz accompanied by spherical divergence correction to enhance the amplitude of signals. The spherical divergence means that the energy loss with an increased depth in the square of the distance. The geometric spreading compensation equation is

$$g(T) = \frac{T^2}{V_0} \cdot g(T_{max})$$

where

T	is time	T_{max}	is maximum time
$g(T)$	is the spreading compensation	V_0	is RMS velocity at zero time

To eliminate low frequency swell noise, we applied low frequency array filtering (0-5 Hz) and noise suppression. Predictive (gap) deconvolution was applied to attenuate near surface multiples (Egbai et al., 2012) with the gap length of 32 ms. To attenuate additional multiple energy, we applied F-K filtering and Radon transforms, including linear and hyperbolic Radon transforms (Fig. 7). In linear Radon transform, the horizontal slowness ($10^6/velocity$) or ray parameter (p) in the time – slowness ($\tau - p$) domain was set and the slowness values range from -116 to 665 s/km for Line E-W and -126 to 665 s/km for Lines N-S.

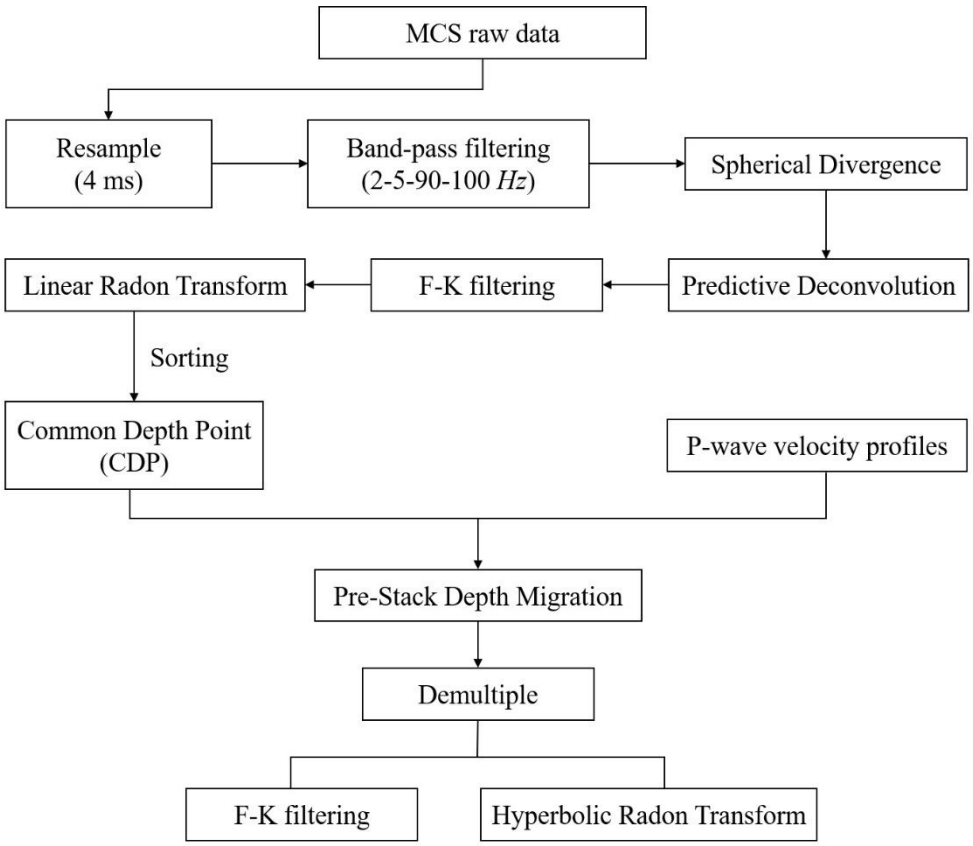

Figure 6 Flow chart showing seismic processing.

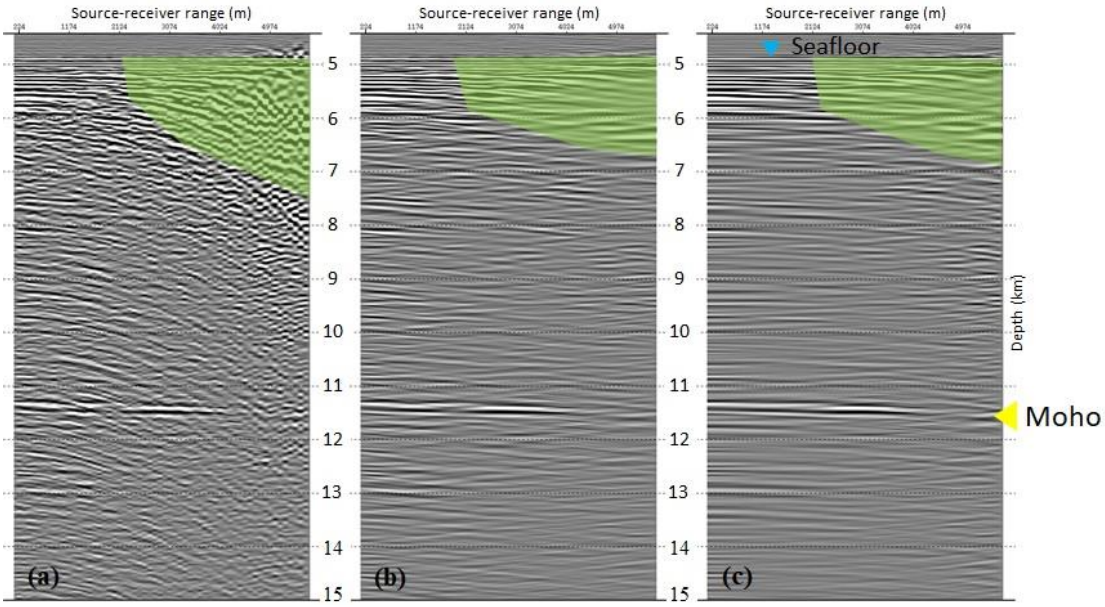

Figure 7 Pre-Stack Depth Gather CDP12571 of Line N-S-2 with (a) linear-Radon transform, (b) F-K filtering and (c) hyperbolic Radon transform in order to remove unwanted hyperbolas in the depth domain after migration. A frequency distortion illustrated in light green polygon is called normal moveout (NMO) stretching. It derives from stretched waveforms in far-offset section (Yilmaz, 2001).

The next important step is velocity analysis. The velocity structure of the oceanic crust (Fig. 8) was computed by JAMSTEC using seismic refraction data from OBSs. We updated the Vp profiles by manually picking the Moho reflections according to maximum amplitude of the strong reflection in Line E-W, Line N-S-1 and Line N-S-2 at 9 - 11 km BSL. Then, we set the velocity at the MTZ to increase from 7.1 to 8.5 km/s, which is supported by the OBS results. The updated velocity (Fig. 9) was applied to image seismic reflection profiles (Fig. 12).

Pre-stack migration is a very accurate and efficient technique in imaging dipping reflectors and non-zero offset traces with high signal-to-noise ratio image (Wu, 2001). Pre-Stack Kirchhoff Depth Migration (PSDM) yields better image than Pre-Stack Kirchhoff Time Migration (PSTM) because PSDM accounts for variation of lateral velocity to correct the lateral shift, while PSTM does not (Yilmaz, 2001; Rosa, 2018). After getting PSDM, we applied F-K and Radon demultiples to attenuate unwanted hyperbolas (Fig. 10).

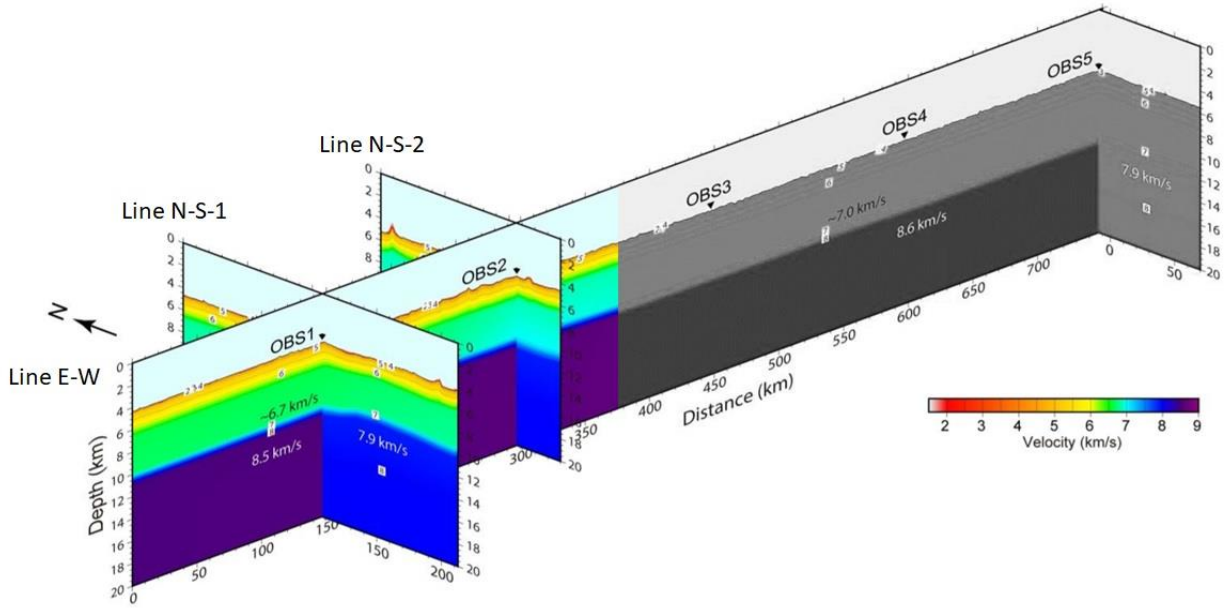

Figure 8 The Vp profiles of Line E-W, Line N-S-1 and Line N-S-2 from Ohira et al., 2018. Data after the first ~350 km of E-W line is outside our consideration in this project.

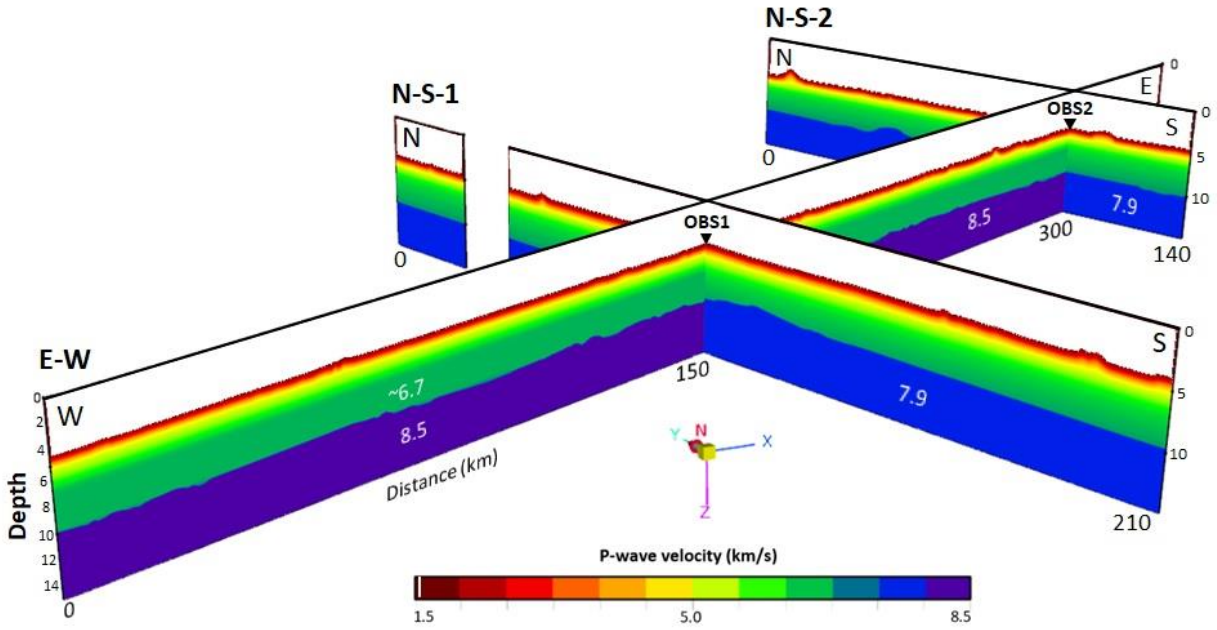

Figure 9 Updated Vp profiles.

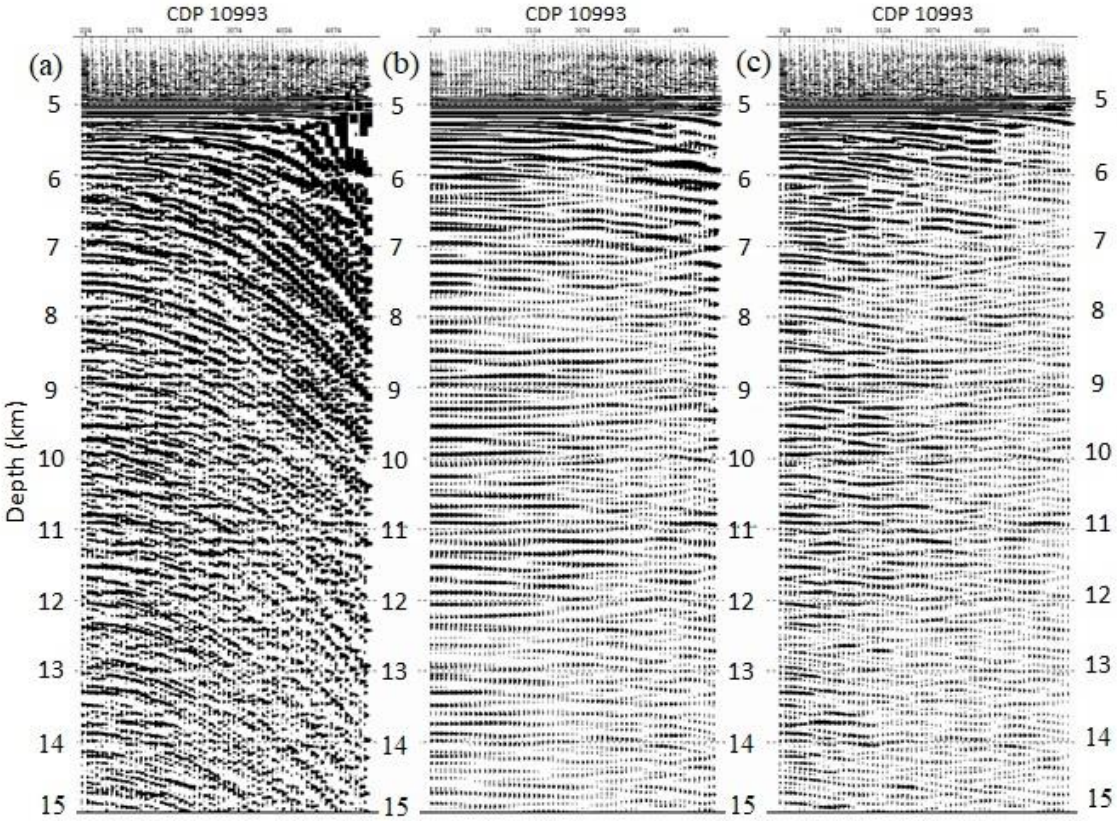

Figure 10 Pre-Stack Depth Gathers (a) without Radon demultiples and F-K demultiples, (b) with Radon demultiples, and (c) with F-K demultiples. The hyperbolas were removed after applying demultiples.

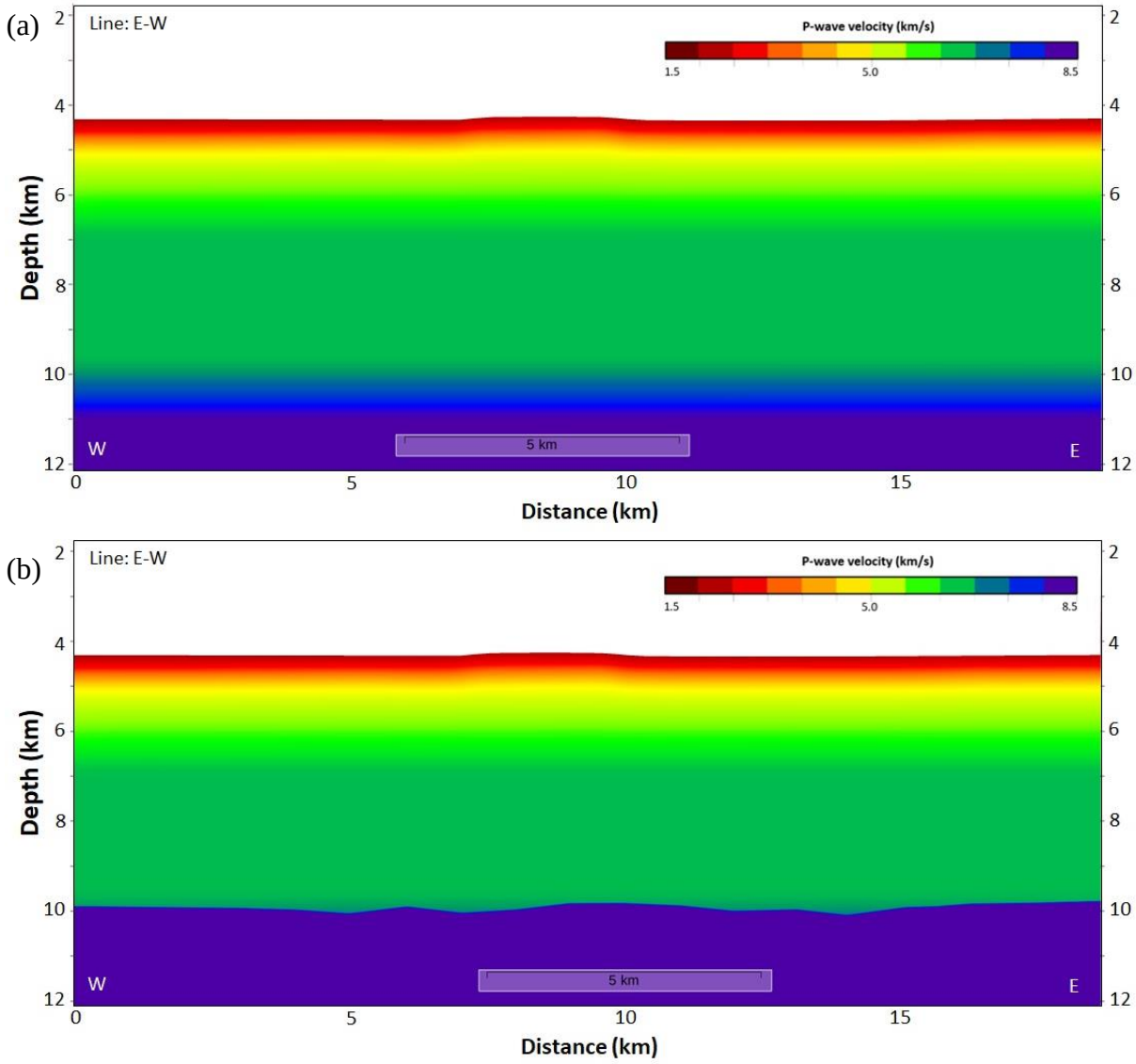

Figure 11 The V_p profiles before updating velocity (a) and after updating velocity (b) in the western section of Line E-W (Fig. 15).

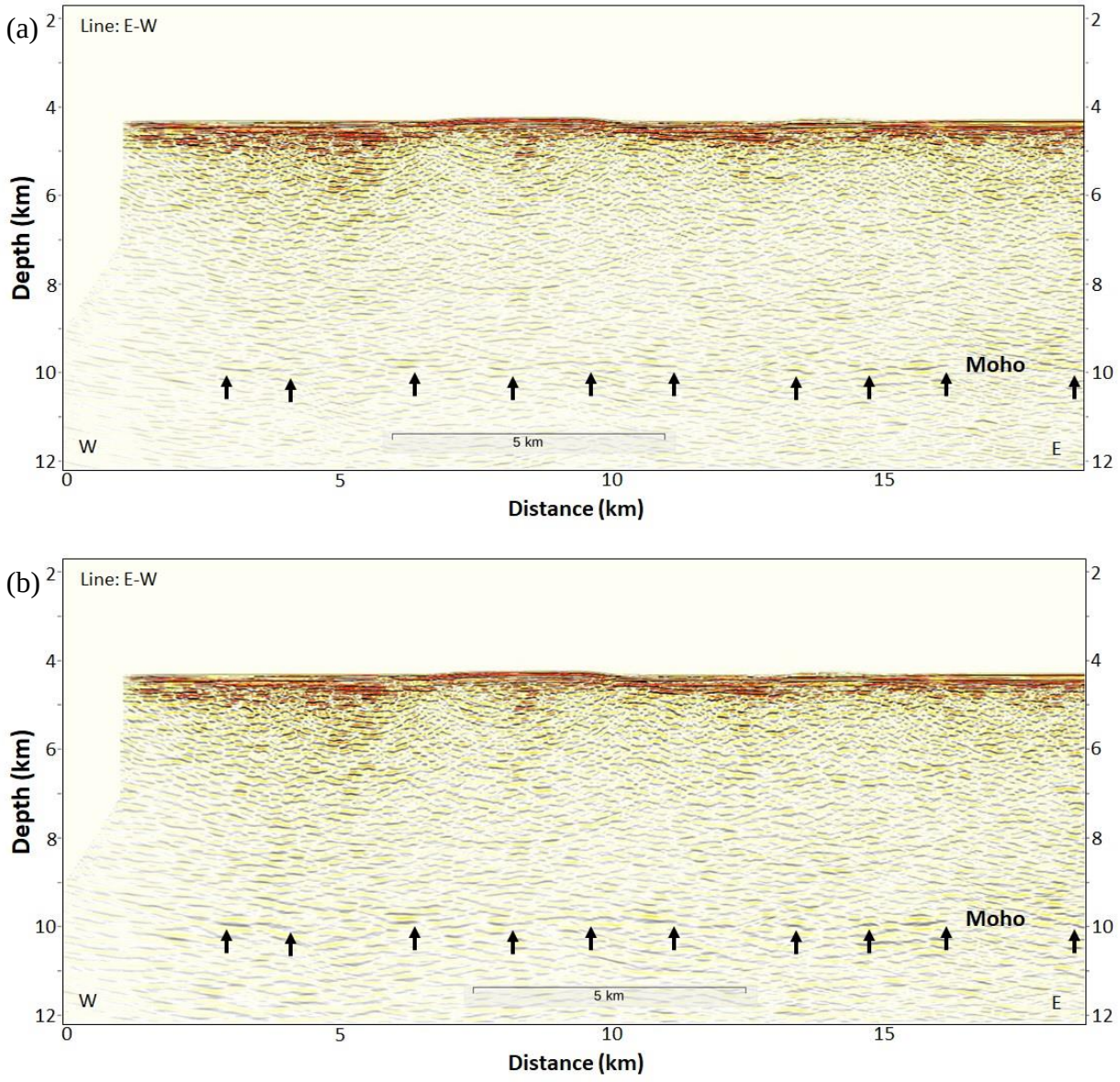

Figure 12 PSDM before updating velocity (a) from Fig. 11a and after updating velocity (b) from Fig. 11b in the western section of Line E-W (Fig. 15). Profile (b) illustrate better image of Moho reflection with higher amplitude than profile (a).

4. Results

The bathymetry along the lines in our survey is smooth and flat with a few small seamounts scattered around the arch (Fig. 13). The series of seamounts follow trend of the Molokai fracture zone. The seafloor depth ranges between 3.7 and 5.2 km BSL. The water depth is shallower southward in Lines N-S and westward in Line E-W.

Three MCS profiles were imaged by using PSDM. We explain the oceanic crustal structure of each line in section 4.1. The survey consists of a long E-W line with two N-S lines which cross at ~150 km (Line N-S-1) and ~300 km (Line N-S-2) from the western edge of Line E-W (Fig. 5 and Fig. 13). The structures of the oceanic crust are divided into three groups, including the upper crust, the lower crust and the Moho which will be explained in section 4.2. In our study, we mainly focus on interesting features located between the lower crust and the Moho.

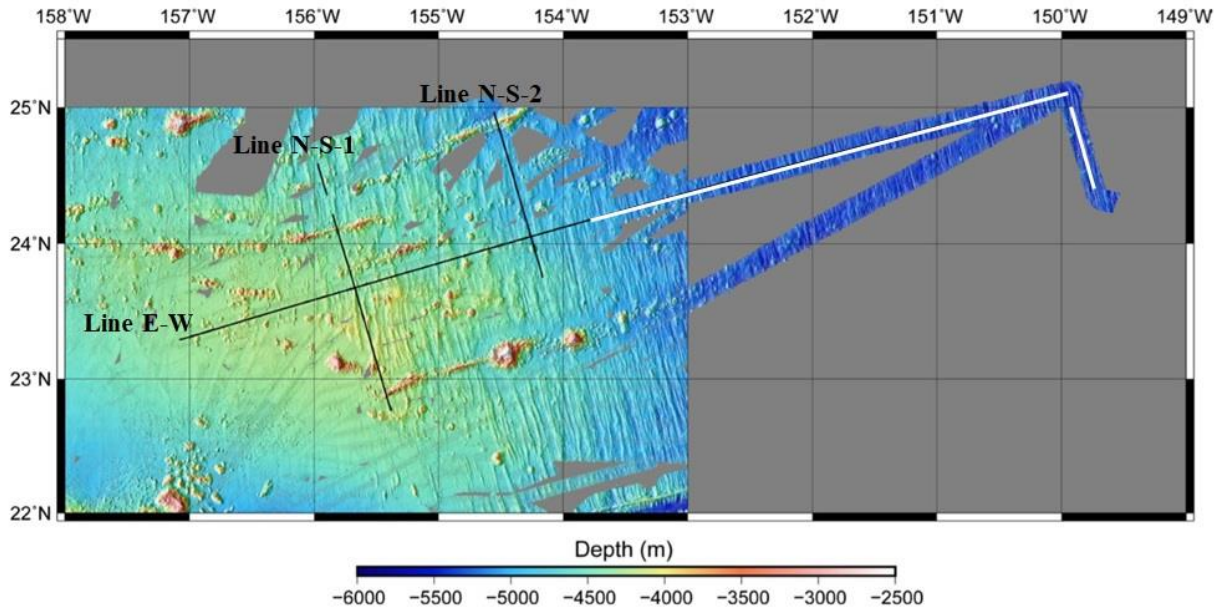

Figure 13 Multibeam bathymetry across the NE Hawaiian Arch (Ohira et al., 2018). The black lines indicate the MCS profiles which we focus on.

4.1 MCS profiles

4.1.1 Line E-W The Moho reflection in Line E-W (Fig. 14) is more clearly seen than Lines N-S (Fig. 15a and Fig. 15b). The Moho reflection is consistent in the western section of the line. Lower crust dipping reflectors (LCDRs) dipped eastward were found in the eastern section of the line and terminated at the Moho (Fig. 21).

4.1.2 Line N-S-1 Lines N-S are parallel to the paleo-ridge axis. There is no visible Moho reflection in the northern section of Line N-S-1. Several high-amplitude seismic reflections were found around the Moho location between 8 and 11 km BSL in Line N-S-1 (Fig. 16). We found LCDRs which are shown in flat events above the Moho reflection. The Moho reflection is located at 9-km depth BSL. We found sub-Moho events (SMEs) between 9 and 11 km BSL.

4.1.3 Line N-S-2 We found the upper crust reflections (UCRs) at ~2 km BSF (Fig. 18c). They are interpreted as the boundary between layer 2 and layer 3. The reflections are shown as small flat segments. The important feature in this line is a dipping Moho reflector (Fig. 17). It dips ~3 degrees from 9 km to 11 km BSL at 54 km north of the intersection of Line E-W. It caused the crust to become thinner in the northern section and thicker in the southern section of dipping. The Moho reflection of thin oceanic crust split into three reflections at 9.5 km BSL (Fig. 17, 22d). We found one SME subparallel to the Moho below the thin oceanic crust.

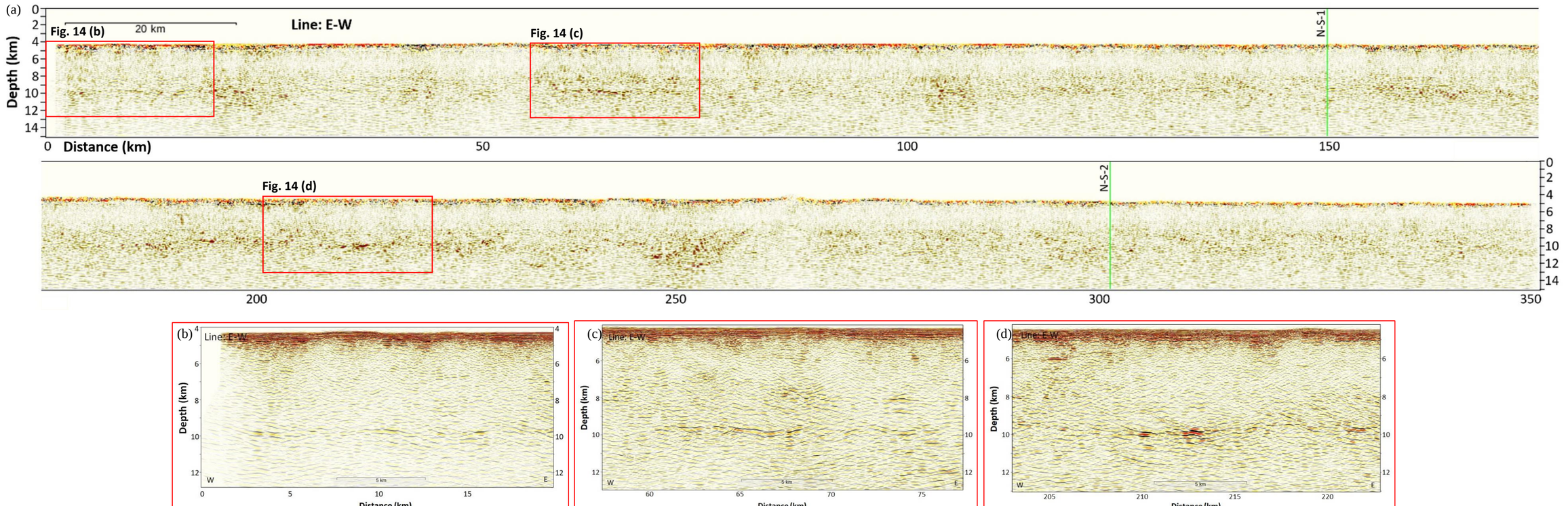

Figure 14 PSDM of Line E-W (a) and zoom-in Moho reflections (b), (c), and (d) with the vertical exaggeration of 2x.

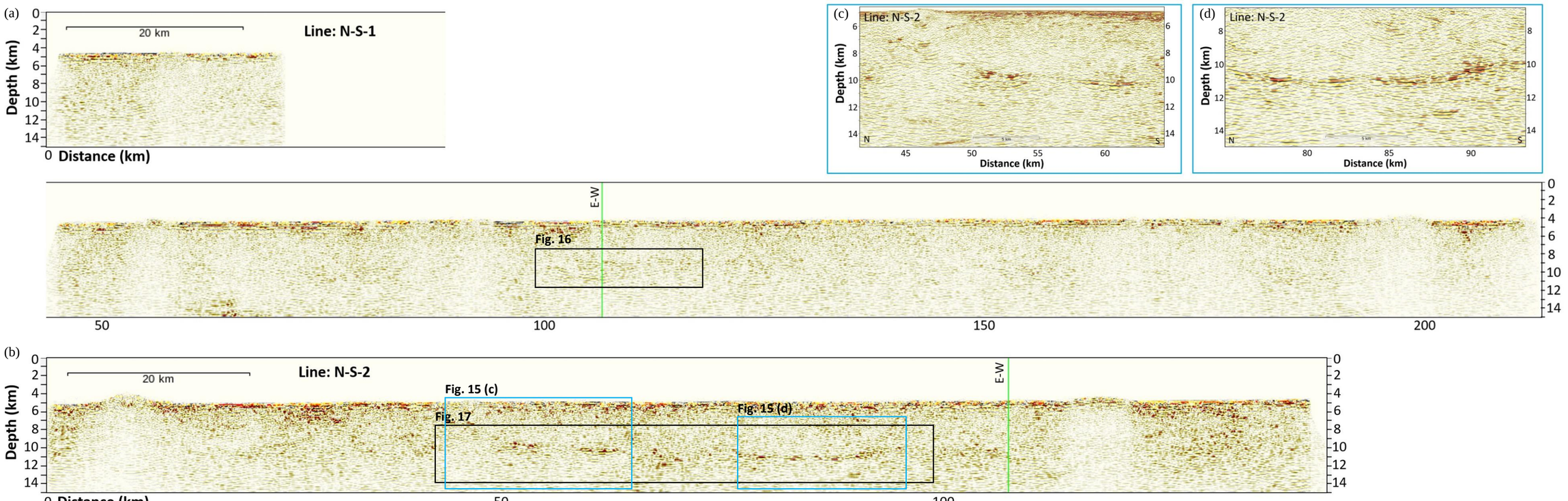

Figure 15 PSDM of Line N-S-1, (a), Line N-S-2, (b), and zoom-in Moho reflections of Line N-S-2, (c) and (d), with the vertical exaggeration of 2x.

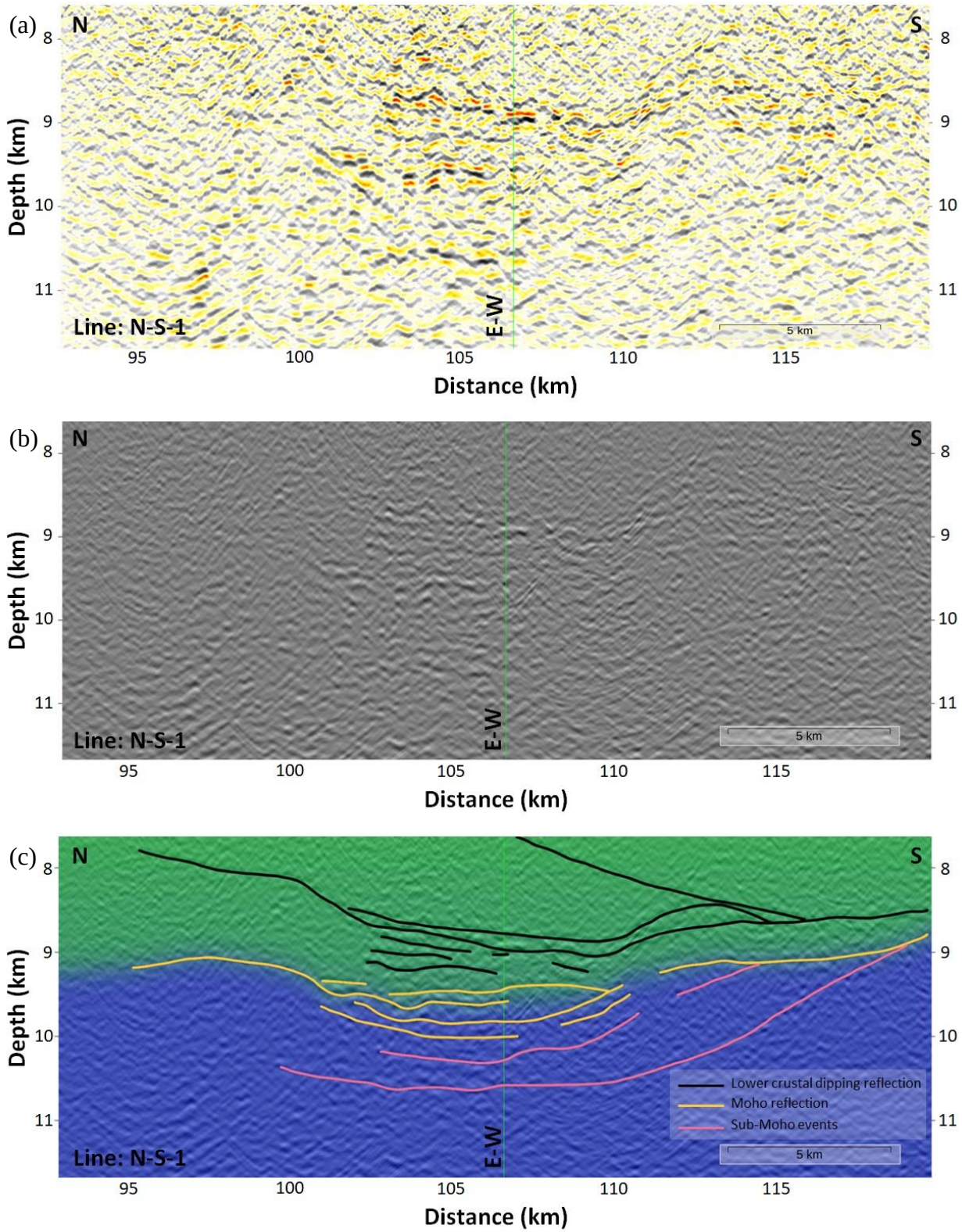

Figure 16 PSDM, (a) and (b), and PSDM superimposed by Vp profile, (c), of Line N-S-1 at the intersection of Line E-W. These images show several high-amplitude reflections around the diffusive Moho, including LCDRs, Moho reflection, and SMEs. The location of these images is shown in Fig. 15a.

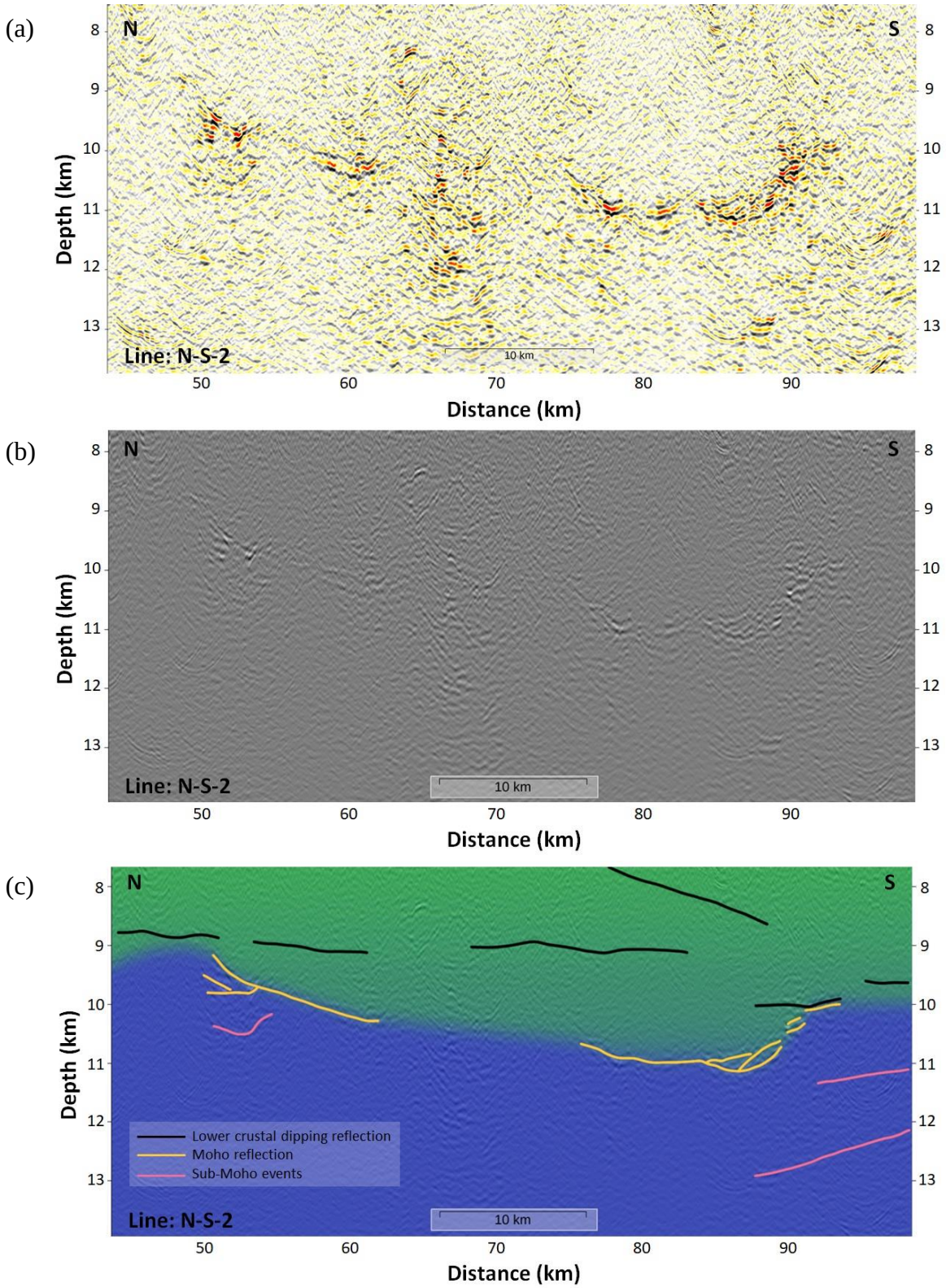

Figure 17 PSDM, (a) and (b), and PSDM superimposed by Vp profile, (c), of Line N-S-2 at 45 km from the north of the line (Fig. 15b). The shallow Moho, thin oceanic crust, splits into three lines at the shallowest point of the Moho depth in Line N-S-2. The black lines indicate LCDRs. Several LCDRs are shown in flat lines above the Moho. The yellow lines indicate the Moho reflection. The pink lines indicate SMEs.

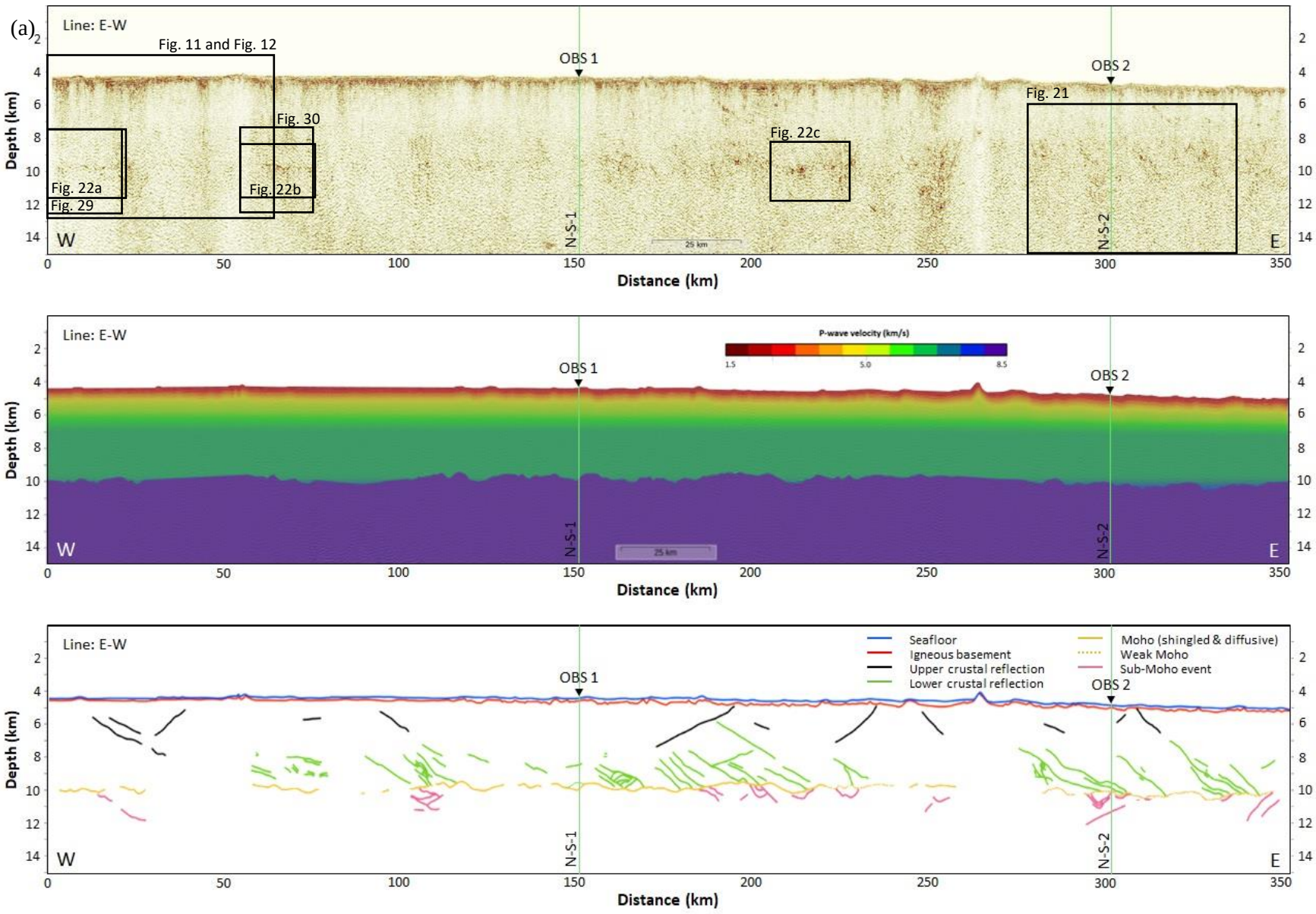
(a)
Line: E-W
Fig. 11 and Fig. 12
Fig. 30
Fig. 22a
Fig. 29
Fig. 22b
Fig. 22c
Fig. 21
OBS 1
OBS 2
N-S-1
N-S-2
W
E
Depth (km)
Distance (km)
P-wave velocity (km/s)
1.5
5.0
8.5
Seafloor
Igneous basement
Upper crustal reflection
Lower crustal reflection
Moho (shingled & diffusive)
Weak Moho
Sub-Moho event

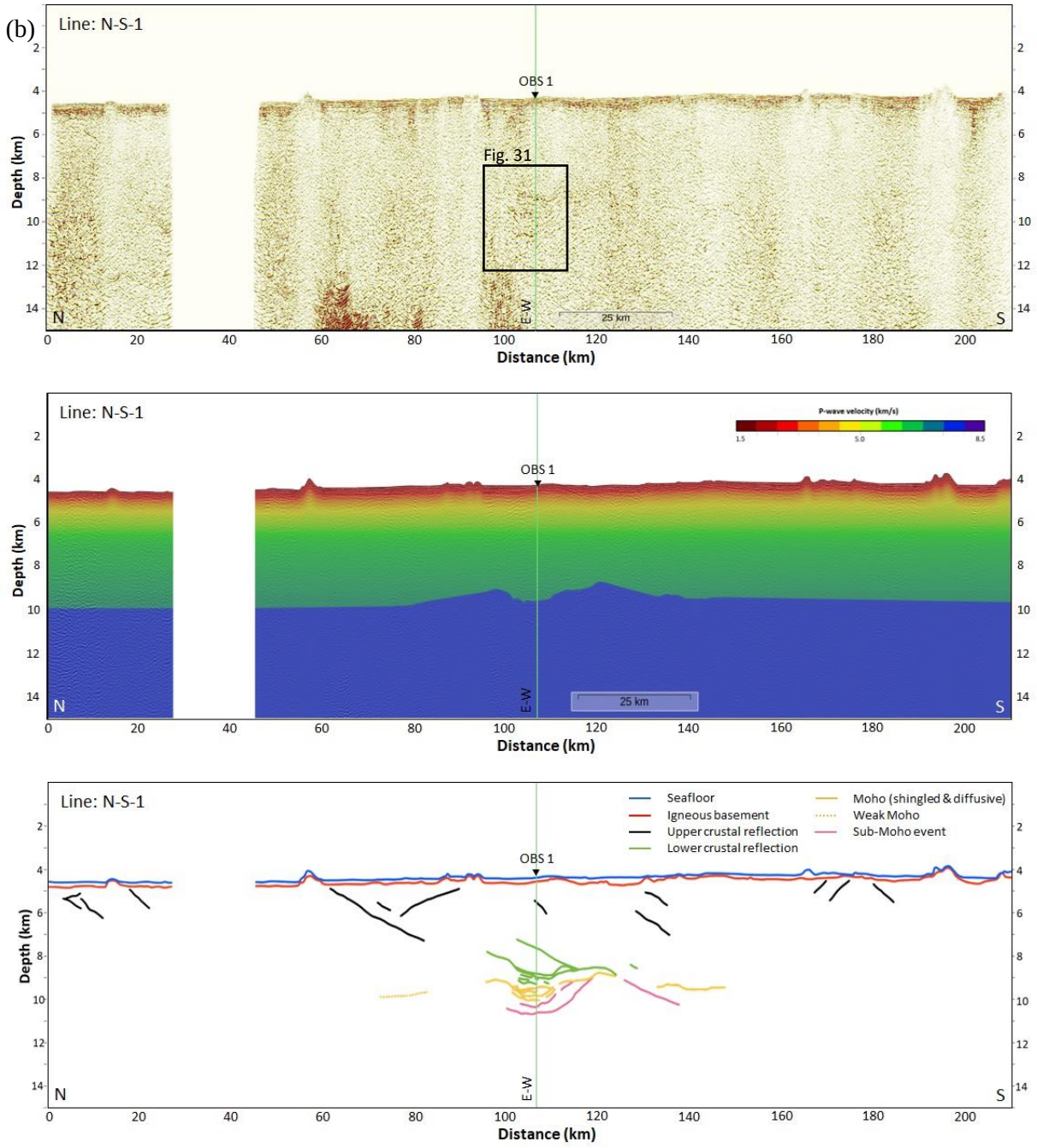
(b)
Line: N-S-1
OBS 1
Fig. 31
Depth (km)
N
S
E-W
25 km
Distance (km)
P-wave velocity (km/s)
1.5
5.0
8.5
Seafloor
Igneous basement
Upper crustal reflection
Lower crustal reflection
Moho (shingled & diffusive)
Weak Moho
Sub-Moho event

(c)

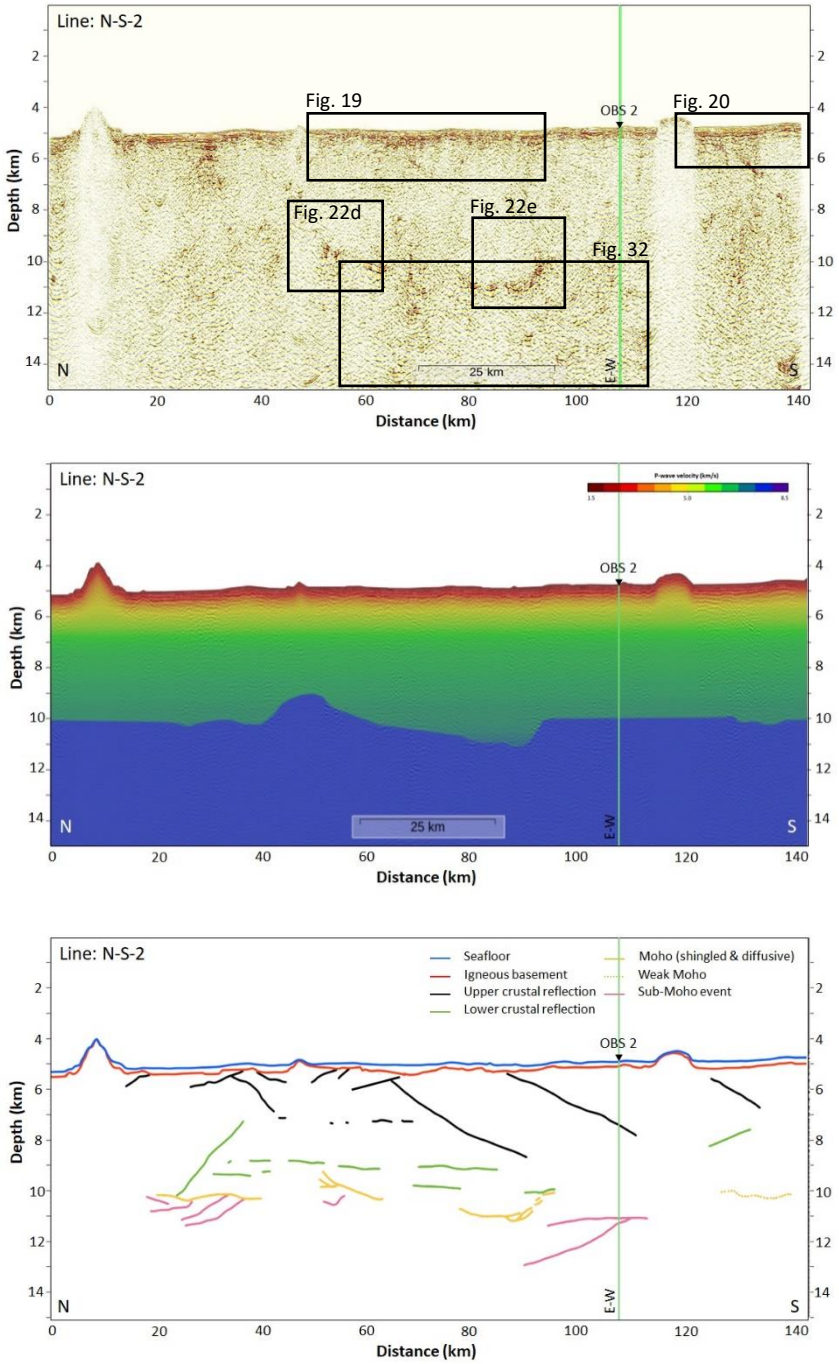

Figure 18 PSDM, Vp profiles and interpretations of all seismic profiles, including Line E-W, (a), Line N-S-1, (b), and Line N-S-2, (c). The blue lines are the seafloor. The red lines are the igneous basements. The black lines are the UCRs. The yellow lines are the shingled or diffusive Moho, while the yellow dots are the weak Moho. The green lines are the lower crustal reflections (LCRs). The pink lines are SMEs. All lines were manually picked by comparing the results from PSDM with and without superimposed Vp profiles.

4.2 Oceanic crustal structure

4.2.1 Sediments, igneous basement and dipping reflections in the upper oceanic crust

The seafloor was covered by pelagic sediments, which are interpreted as brown clay (Fan and Grunwald, 1971). Although the seafloor is flat, the igneous basement is not smooth because of the growth of seamounts (Fig. 19). The sediments are very thin above seamounts and can be as thin as 7 m. The average sediment thickness from the data extracted every 1-km is approximately 200 m (Table 3). We found upper crust dipping reflections (UCDRs) in Line N-S-2 (Fig. 20). They did not pass through the igneous basement. Their lengths range from 9 to 26 km.

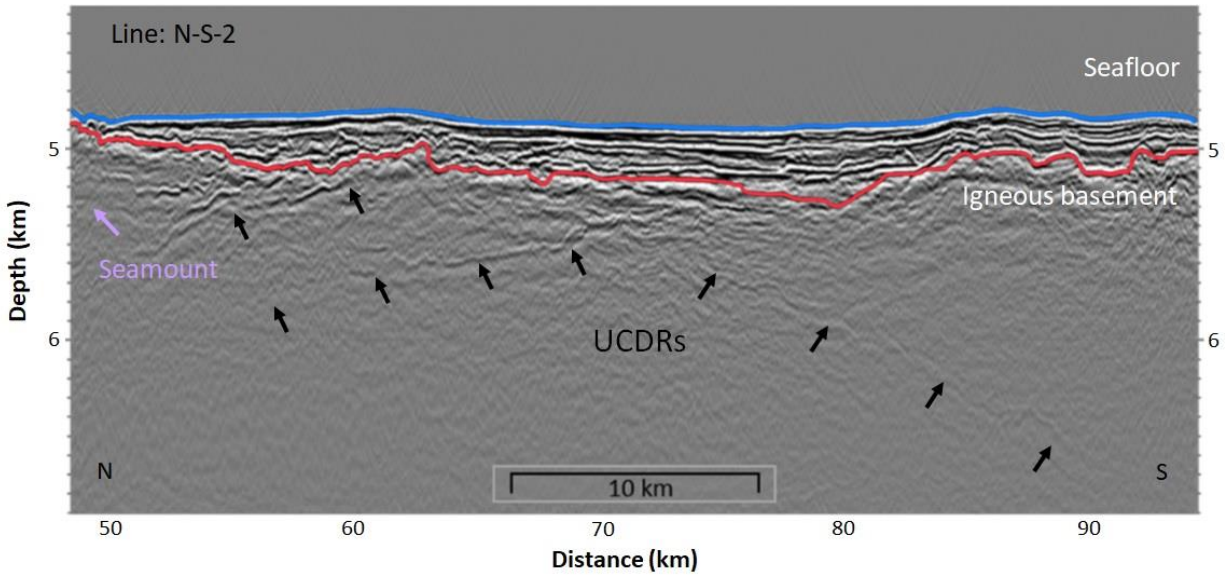

Figure 19 PSDM of the upper crust of Line N-S-2 at 50 km from the northern edge of the line (Fig. 18c). The blue and red lines indicate the seafloor and igneous basement, respectively. A seamount was located at the northern side of this image. The black arrows indicate the UCDRs. We found several smalls UCDRs which dip toward the seamount.

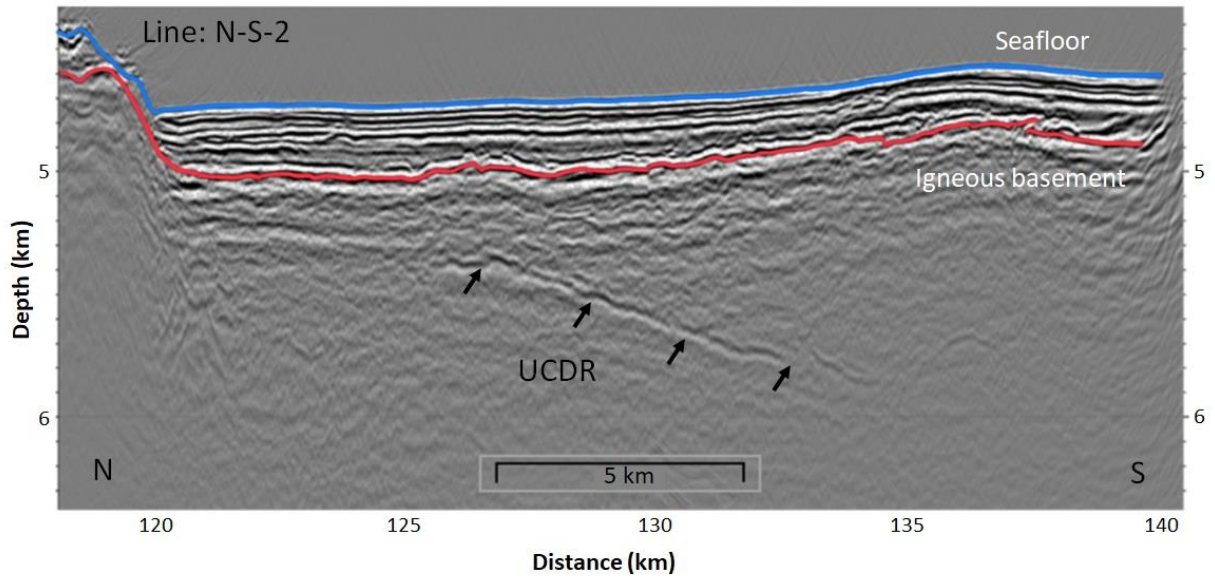

Figure 20 PSDM of Line N-S-2 in the southern section of the line (Fig. 18c). The sediment layers are laminated with constant thickness in this area. In this image, the southward dipping reflection of the UCDR dips 9 degrees.

Table 3 Thickness of sediment layers and depth of seafloor in all seismic reflection profiles

Line	E-W		N-S-1				N-S-2	
			N-S-1 (1st)		N-S-1 (2nd)			
	SF	Sed	SF	Sed	SF	Sed	SF	Sed
min	3961	15	4406	41	3709	7	3806	37
max	4995	371	4595	307	4516	473	5141	490
mean	4421	187	4562	201	4269	179	4835	225

*SF = depth of seafloor (MBSL) and Sed = thickness of sediment layers (m).

4.2.2 Lower crustal dipping reflection (LCDRs) In Line E-W, eastward dipping reflections (Fig. 21) are found beneath rather smooth seafloor in the eastern section of Line E-W and dip toward the paleo-ridge axis at 5 to 12 degrees. The average length of LCDRs is ~11 km long starting at ~3 km BSF in layer 3, which is the gabbro layer. The length of LCDRs ranges between 3 and 24 km. They terminate at the Moho, ~5.4 km BSF,

and are shown with irregular intervals. We found LCDRs as flat events in Line N-S-2 that is parallel to the paleo-ridge axis.

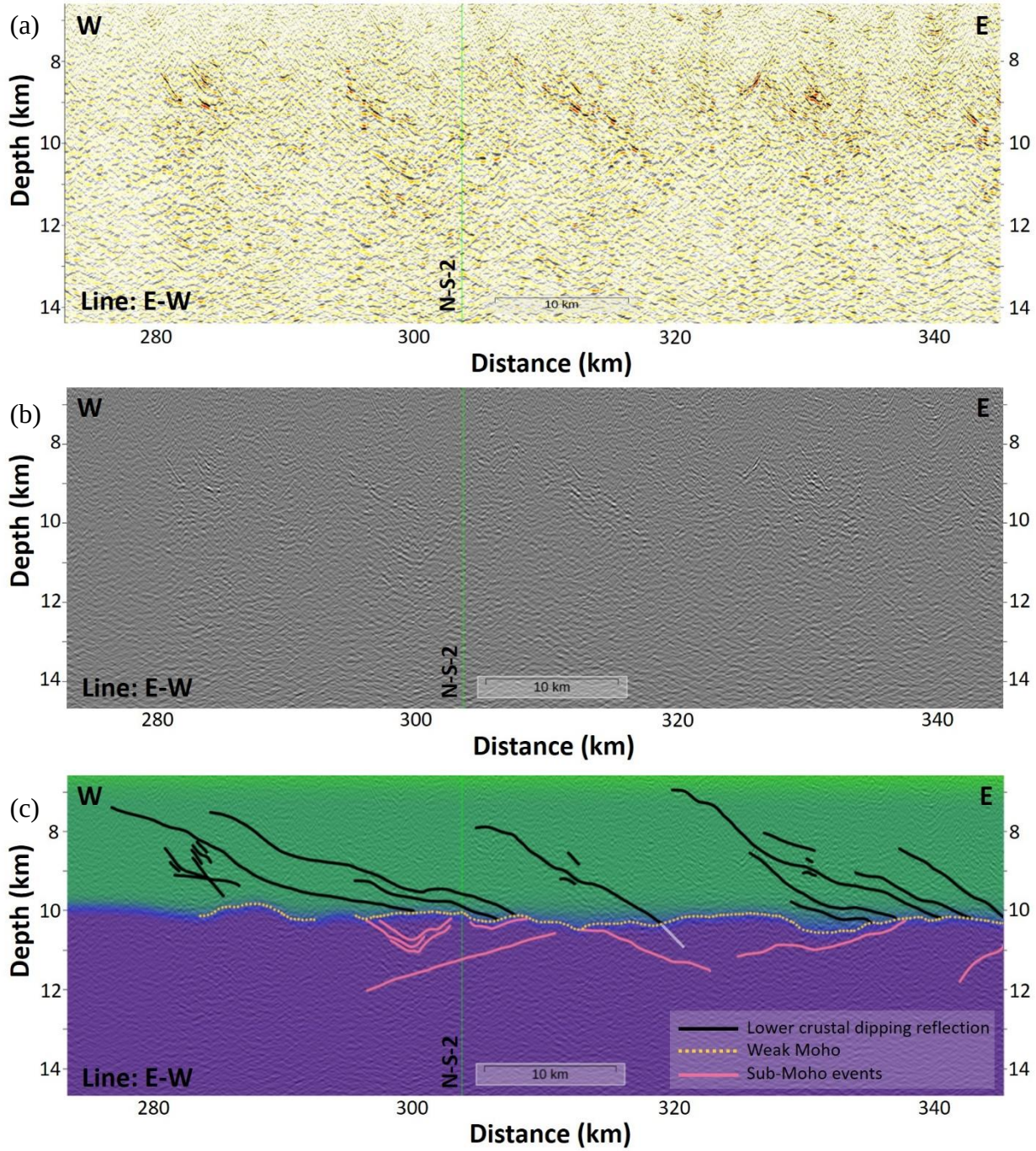

Figure 21 PSDM, (a) and (b), and PSDM superimposed by Vp profile, (b), of Line E-W at the intersection of Line N-S-2 in the eastern section of Line E-W (Fig. 18a). The black lines indicate LCDRs. The pink lines indicate SMEs. A LCDR is continuous to one reflection, which is illustrated by the white line, and deepen to 11 km BSL, crossing the Moho reflection. This reflection was suspected to be an artifact of incomplete migration, undermigration (e.g. Reston et al., 1999).

4.2.3 Moho characteristics The Moho reflections in our study have variable characteristics. The Moho is not well-defined along all of the lines. We observe the shingled and diffusive Moho, which vary between 4.3 to 6.3 kilometers BSF. The Moho reflections are imaged within ~50% of all survey lines, including 5% of the shingled Moho and 45% of the diffusive and weak Moho. The Moho shapes are flat, curved, and mounded (Fig. 22). The Moho reflections are weak in the eastern section of Line E-W and absent beneath a rough igneous basement, especially under seamounts. The rough igneous basement can cause acoustic energy scattering (Nedimovic et al., 2005) which can produce thick MTZs (>100m; Jousselin and Nicolas, 2000) due to a gradually increased ratio of thin alternating dunite and gabbro sills with depth (Nedimovic et al., 2005). The MTZs change in velocity within <1 km.

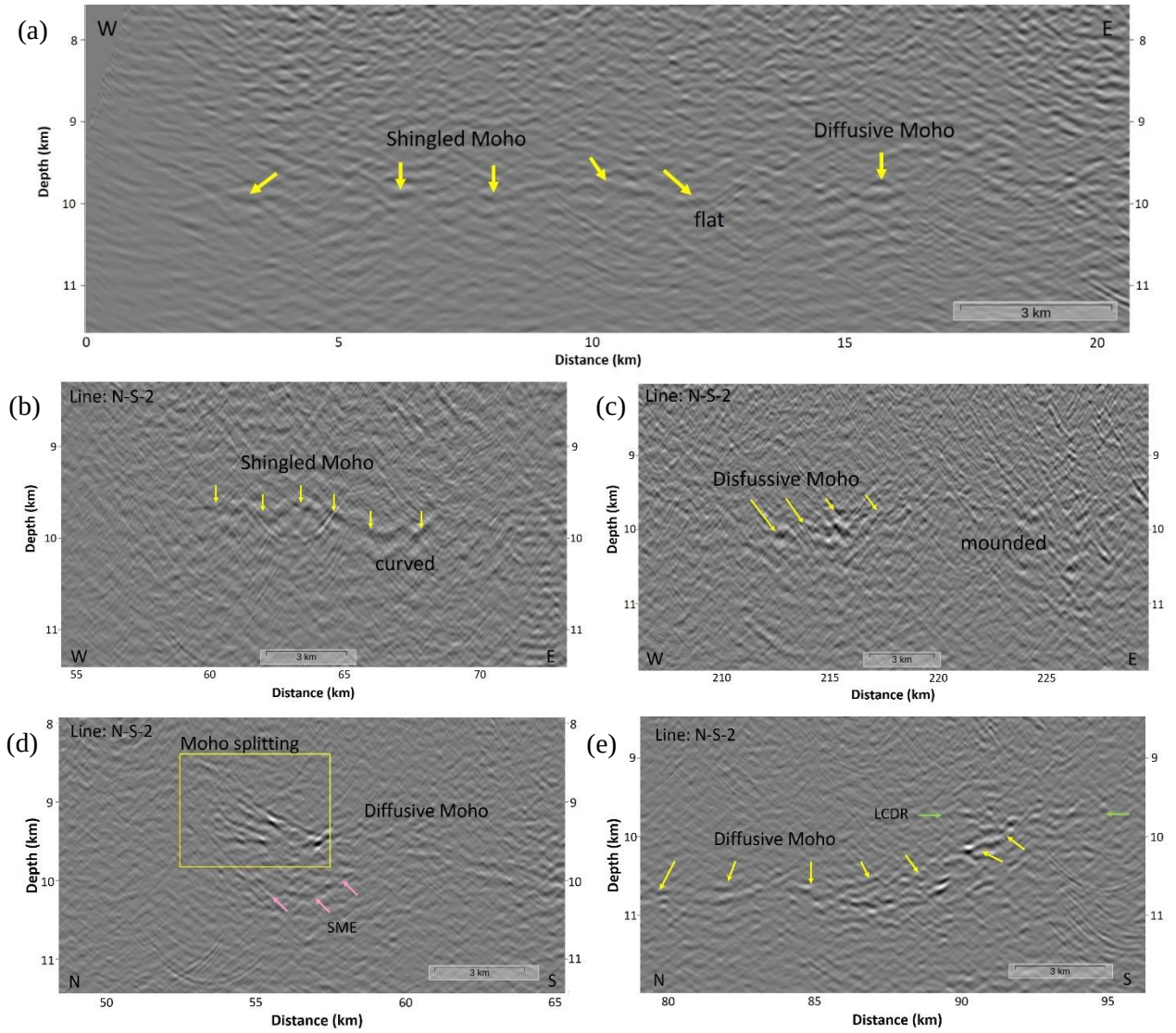

Figure 22 Different shapes of Moho reflections between 8 to 11 km BSL. (a), (b) and (c) are from Line E-W; (a) and (b) are in the western section of the line, and (c) is at 63 km east of the intersection of Line E-W and Line N-S-1 (Fig. 18). (a), (b) and (c) are detected at ~5.5 km BSF. (d) and (e) are from Line N-S-2 located in the center of the line (Fig. 18c). The yellow arrows indicate the Moho reflections. The pink arrows indicate SME. The yellow rectangle indicates the Moho splitting.

4.2.4 Depth of the Moho The Moho depth was computed by including the depth of the water column and oceanic crust. The Moho depth at the 80-Ma oceanic crust in Line N-S-1 is ~9 km BSL, which is the shallowest Moho depth. The deepest Moho is ~11 km BSL located in Line N-S-2. Due to the bending of 86-Ma Pacific plate, the oceanic crust was pushed up 200 m in order to balance the Hawaiian volcanic loading which formed the arch. The Moho is shallow at the arch. Although the Moho depth fluctuates across the arch, the trend of the Moho depth is deeper toward the east until ~10 km BSL at the eastern edge of Line E-W.

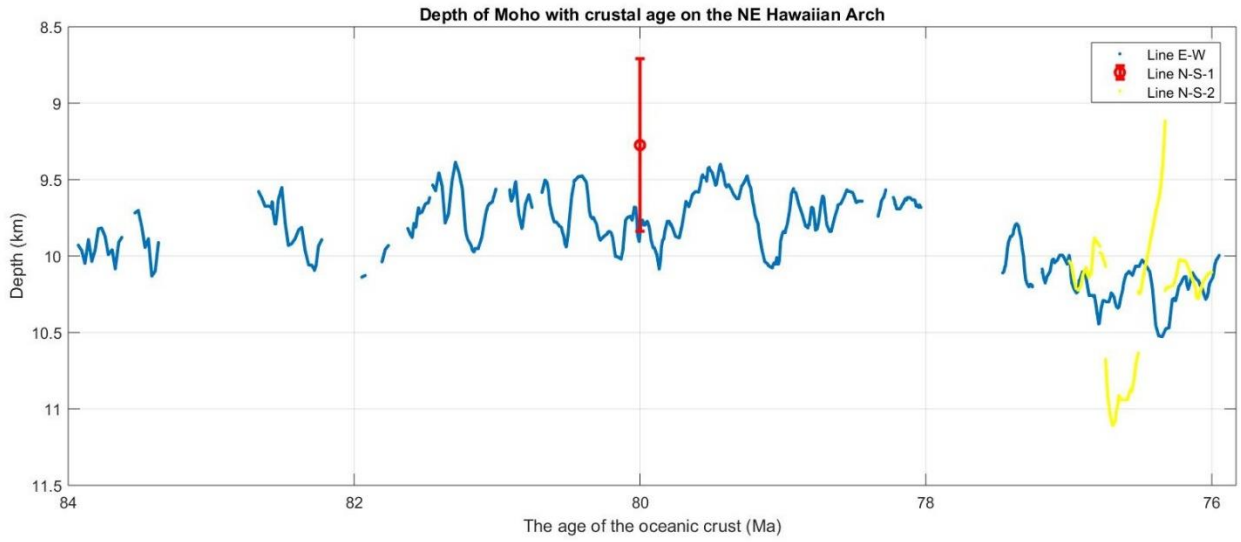

Figure 23 Correlation of Moho depth with oceanic crustal age. The blue, red and yellow dots indicate the crustal thickness in Lines E-W, N-S-1 and N-S-2, respectively. The age of oceanic crust in Line E-W ranges between 76 and 84 Ma. The age of oceanic crust in Line N-S-1 is ~80 Ma, while the age of oceanic crust in Line N-S-2 ranges from 76 to 77 Ma.

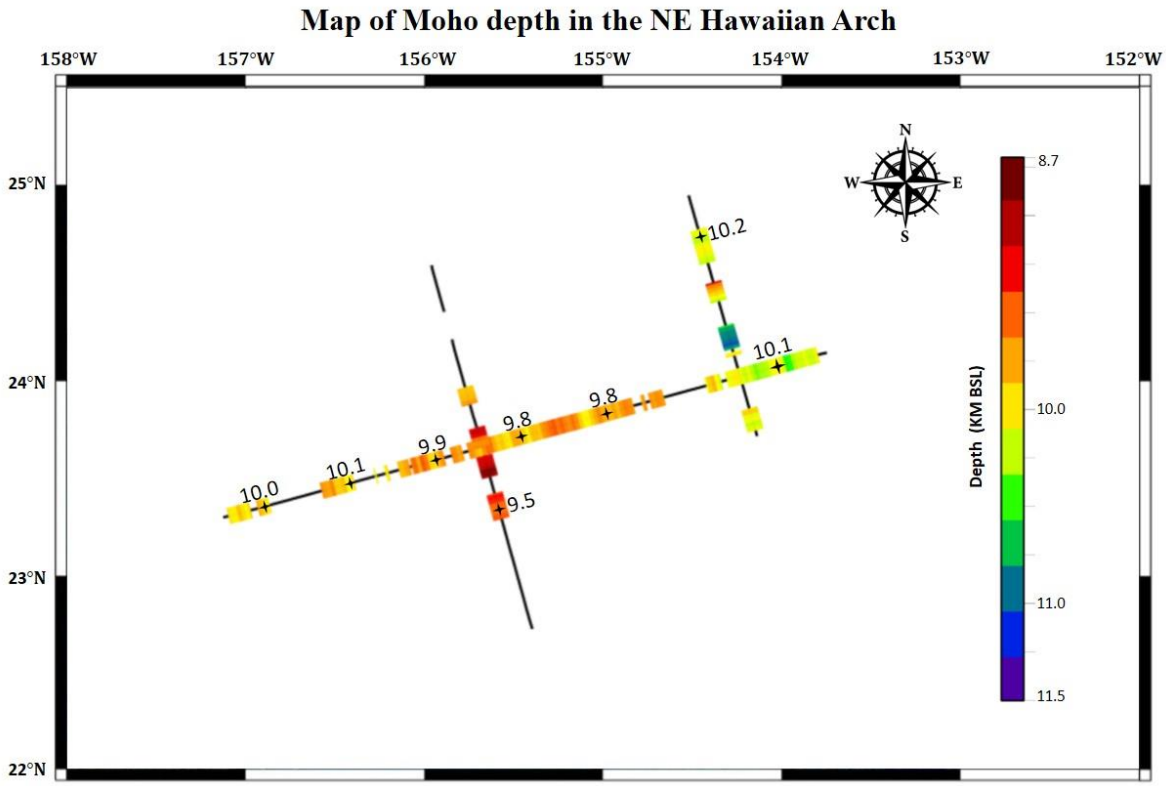

Figure 24 Moho depth in the NE Hawaiian Arch.

5. Discussion

5.1 P-wave velocity profiles

The V_p at the Moho in Line E-W changes from ~7 to 8.5 km/s at the arch and 8.6 km/s at the back of the arch, or the basin (Fig. 8). The V_p in layer 3, layered gabbro, at the basin is also higher than over the arch. Ohira et al. (2018) suggested that reduced velocity between the arch and the basin might be related to the bending of lithosphere, which increases extensional strains and crack opening. The velocity at the Moho on Lines N-S increases from ~7 to 7.9 km/s, which is much lower than the velocity on Line E-W. The different velocity between the MCS lines parallel to the paleo-ridge axis, Lines N-S, and the transverse line, Line E-W, leads to the strong degree of anisotropy (DA). It is ~9% beneath the Moho (Ohira et al., 2018), which agrees with the value of

8.5 - 9.8% reported for the northwestern Pacific, off the Kuril Trench, by Kodaira et al. (2014). Their V_p immediately below the Moho changes to 8.5 - 8.6 km/s in the profile oriented perpendicular to magnetic anomaly and 7.8 km/s in the perpendicular profile. Kodaira et al. (2014) and Ohira et al. (2018) reported that the strong azimuthal seismic anisotropy in the upper mantle arose from an alignment of olivine crystal in heterogeneous materials, which was induced by mantle flow around the paleo-spreading center. Plate motion and mantle density heterogeneity also contribute to DA in the oceanic crust (Conrad et al., 2007). Increased velocity of the Pacific plate motion directly varies with enlarged shear in the upper mantle which induces strengthened anisotropy (The MELT Seismic Team, 1998).

5.2 Origins of lower crustal dipping reflections

LCDRs possibly arise from post accretion process, lithological fabric, and shear zones (Reston et al., 1999; Kodaira et al., 2014; Bécel et al., 2015).

LDCRs can originate by post crustal accretion processes such as brittle faulting, fracturing and off-axis magmatism. They disappear in the oceanic crust near the mid-ocean ridge or younger than 5 Ma (Hallenborg et al., 2003). They create offsets either at the igneous basement or the Moho. The alteration of minerals and fluid trapped at these off-axis processes can create a contrast of acoustic impedance (Jones and Nur, 1984). If faults penetrate deep into the lower crust, these structures can induce deep hydration and off axis illumination (Bécel et al., 2015) of the oceanic lithosphere. The LCDRs in our observation do not reach to the igneous basement and terminate at the Moho. There is no offset found at the top of oceanic crust and/or the MTZ, so our data are not supported by this origin.

The second possible explanation for LCDRs is lithological layering (e.g. Reston et al. 1999) with a gabbro-glacier accretion model which was used to illustrate the formation of the lower crust. When the axial magma chamber produces molten or partially molten materials, they flow downward and outward and ridgeward-dipping reflectors are formed continuously (Morgan and Chen, 1993; Nicolas, 1994). In this case, LCDRs should flatten into the Moho. LCDRs in our data are discrete features and do not flatten downward to the Moho. They are in disagreement with the process of lithological layering.

LCDRs could originate from secondary shear zones in response to active mantle flow where the uppermost mantle moves away from the spreading center faster than the crustal spreading rate (Kodaira et al., 2014; Bécel et al., 2015). These LCDRs were formed at fast-spreading rates, such as the Pacific plate between the Kuril Trench and Shatsky Rise as well as south of the Aleutian Peninsula, similar to our study area (Kodaira et al., 2014; Bécel et al., 2015). Bécel et al. 2015 reported that melt concentration within shear zones can generate strong seismic reflections. They are expected to be imaged as LCDRs that flatten upward (Reston et al., 1999). The secondary shear zones due to a basal drag force of an active magma upwelling at mid-ocean ridge may be used to explain the origin of LCDRs in our data.

5.3 Moho discontinuity and sub-Moho structure

The remarkable feature in this study is wavy Moho in Line N-S-1 (Fig. 16). The wavy Moho is interpreted as a diffusive Moho. We found SMEs below the wavy Moho which are interpreted as a small magmatic intrusion, approximately half km wide, at the intersection of Line E-W and Line N-S-1 (Fig. 25). SMEs were also found in all lines and normally accompanied with the diffusive Moho. In an ideal case of a simple sill intrusion, the reflections would show the

discrimination between positive and negative polarities at the top and the bottom of sill intrusion (Singh et al., 1998; Nedimovic et al., 2005). However, the SMEs might not illustrate the discrimination of two-polarity impedance contrast if there are more than one sill at the MTZ. Nedimovic et al. 2005 reported that the emplacement of gabbroic lenses and melt accumulation in residual peridotite are commonly seen beneath fast- to intermediate-spreading centers, but sill intrusion can be preserved if it formed at the propagator tips which is different geological setting to the crustal accretion processes of our study area. In our observation, we cannot identify the origins of these SMEs.

Another prominent feature is the deep Moho, or the thick oceanic crust which is as thick as ~6.3 km, found in Line N-S-2 (Fig. 15d, 17 and 22e) and the shallow Moho, or the ~4.3-km thin oceanic crust, found at north of the thick oceanic crust (Fig. 15c, 17 and 22d). The discrepancy of crustal thickness possibly associates with the seafloor spreading rate and the age of oceanic crust (McKenzie et al. 2005). Increasing the degree of partial melting may cause thickening of the crust (Reston et al., 1999).

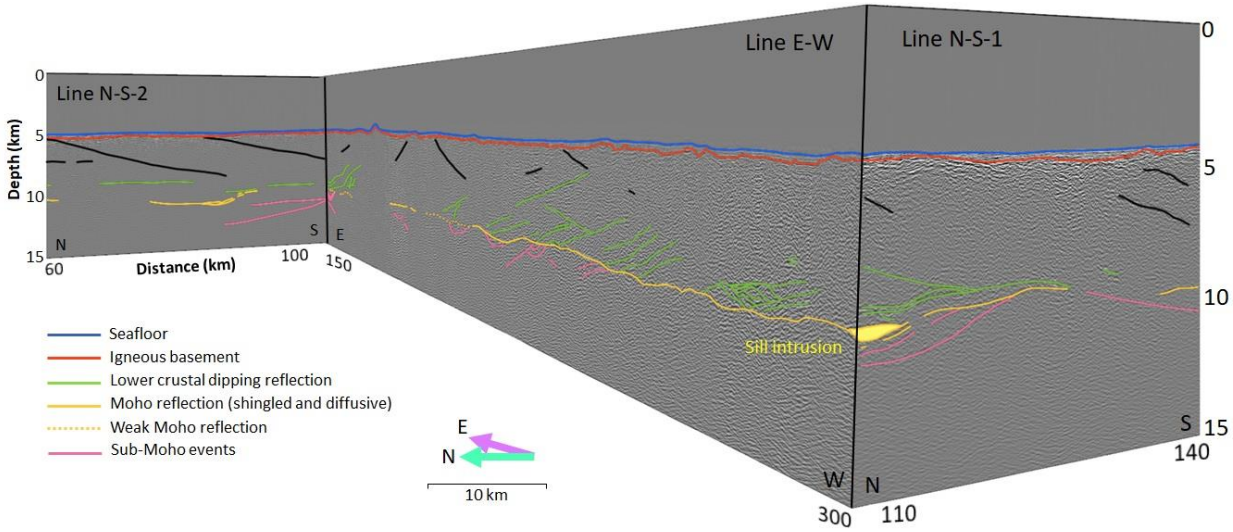

Figure 25 The intersection of Line E-W, Line N-S-1 and Line N-S-2. We interpret the yellowish area as sill intrusion.

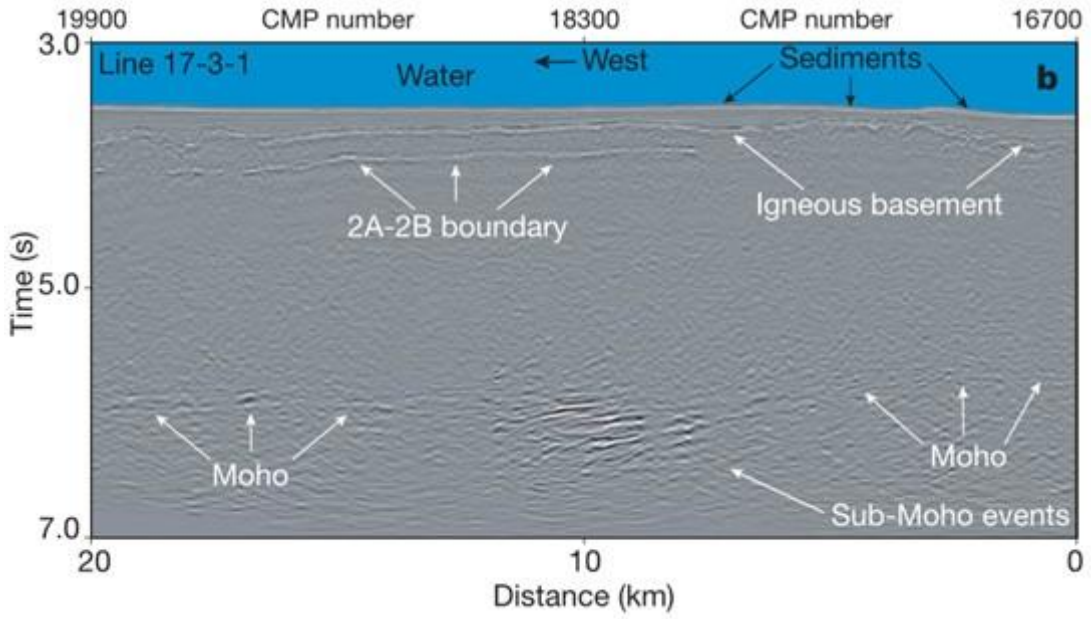

Figure 26 Example of sill intrusion. The series of SMEs found beyond the ridge axis of Juan De Fuca >~20km are indicative of gabbro-melt sills within a thick MTZ (Nedimovic et al., 2005).

5.4 The oceanic crustal thickness of our study in comparison to other surveys

The crustal thickness is measured as the distance between the seafloor and the Moho. The average crustal thickness in our study area is approximately 5.4 km with a standard deviation (σ) of 0.3 km. It varies from 4.3 to 6.3 km. The average crustal thickness of Line E-W is 5.4 km with σ = 0.2 km. In Line N-S-1, the average crustal thickness is 5.2 km with σ = 0.3 km. In Line N-S-2, the average crustal thickness is 5.4 km with σ = 0.4 km. The thickness of oceanic crust of our study is plotted with other records in the Pacific Ocean (Fig. 27). Although the oceanic crust in our study area is affected by the flexural bending, the thickness of oceanic crust is shown corresponding with the recorded data from Van Avendonk et al. (2017).

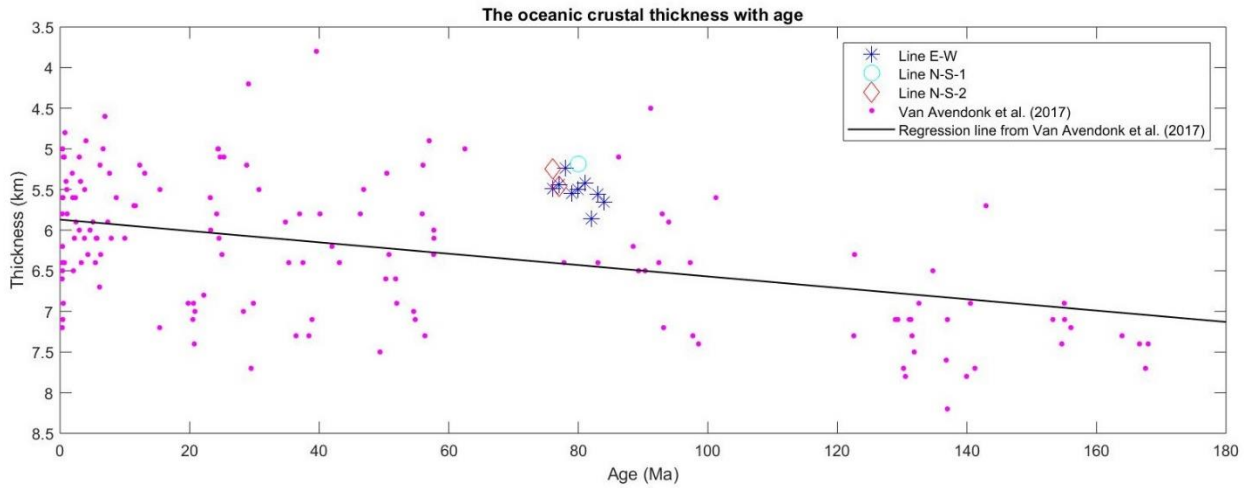

Figure 27 Correlation between oceanic crustal thickness and plate age. The crustal age shown in graph (a) ranges from 0 to 180 Ma. The magenta dots indicate the thickness of oceanic crust in the Pacific Ocean basin from Van Avendonk et al. (2017). The blue asterisks indicate the crustal thickness of Line E-W. The cyan circle indicates the crustal thickness of Line N-S-1. The red diamonds indicate the crustal thickness of Line N-S-2. The black line is the linear regression of the crustal thickness in the Pacific Ocean basin.

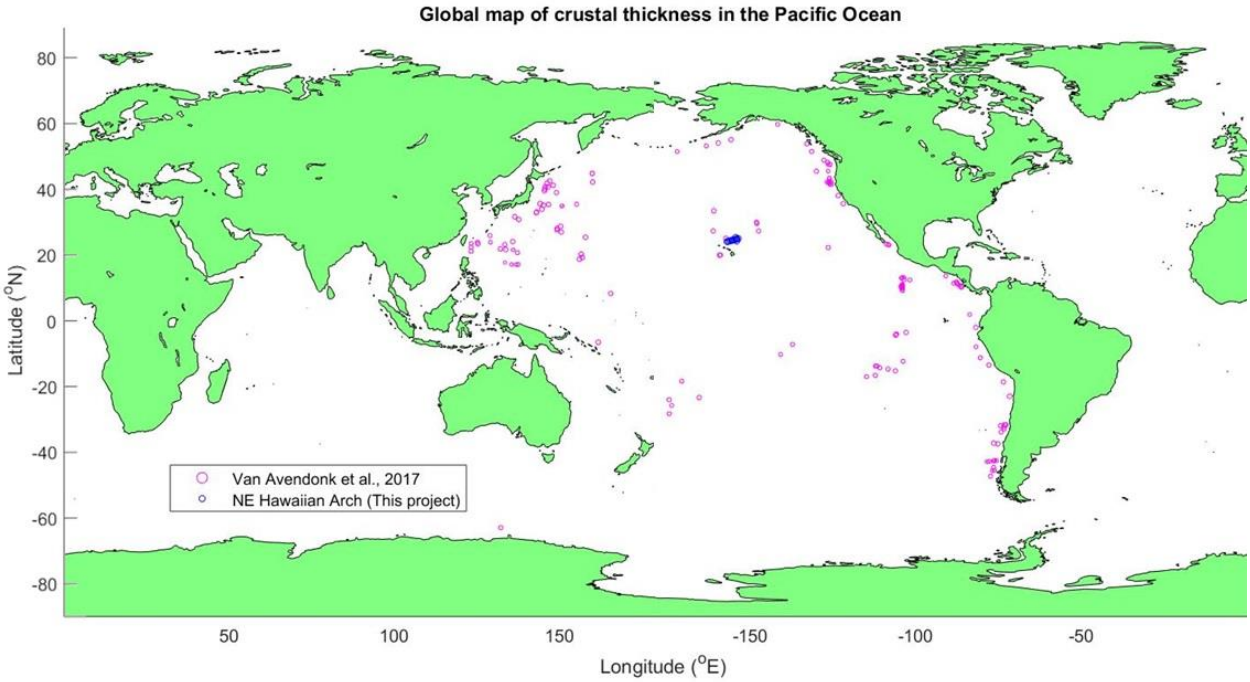

Figure 28 Global map of crustal thickness in the Pacific Ocean from Van Avendonk et al. (2017) and this study. The magenta and blue circles indicate the locations of crustal thickness (Fig. 27) from Van Avendonk et al. (2017) and this study, respectively.

5.5 Comparison to the previous interpretation of this data set

Ohira et al. (2018) processed the same MCS profiles using different modules in Paradigm software. The steps of their seismic reflection processing consisted of band-pass filtering, trace editing, F-X deconvolution, fan filtering, tau-p deconvolution, amplitude recovery and predictive (gap) deconvolution. After applying velocity profiles and stacking, they conducted Post-Stack Kirchhoff time migration (Post-STM), Radon demultiple, Automatic Gain Control, and muting. Depth conversion was applied to get the final post-stack migration in depth domain.

Although the post-stack migration by Ohira et al. 2018 produced a sharper seismic imaging than our results, the Moho reflection responses and subcrustal structure were better imaged in our study using PSDM. We compared the structures of the lower crust and the upper mantle between Ohira et al. 2018 (Fig. 29a – 32a) and our PSDM results (Fig. 29b - 32b). We identified the shingled Moho at the western edge of Line E-W, 5.7 km BSF (Fig. 29), where the Moho is separated into segments ~21.7 km long. Another shingle Moho was found at 60 km from the western edge of Line E-W, 5.5 km BSF (Fig. 30). Its length is 17.5 km. In Line N-S-1, a prominent Moho was visibly detected in our result (Fig. 31b). We also found SME in Line N-S-2 (Fig. 32b). No evidence of magmatic underplating was seen in either study.

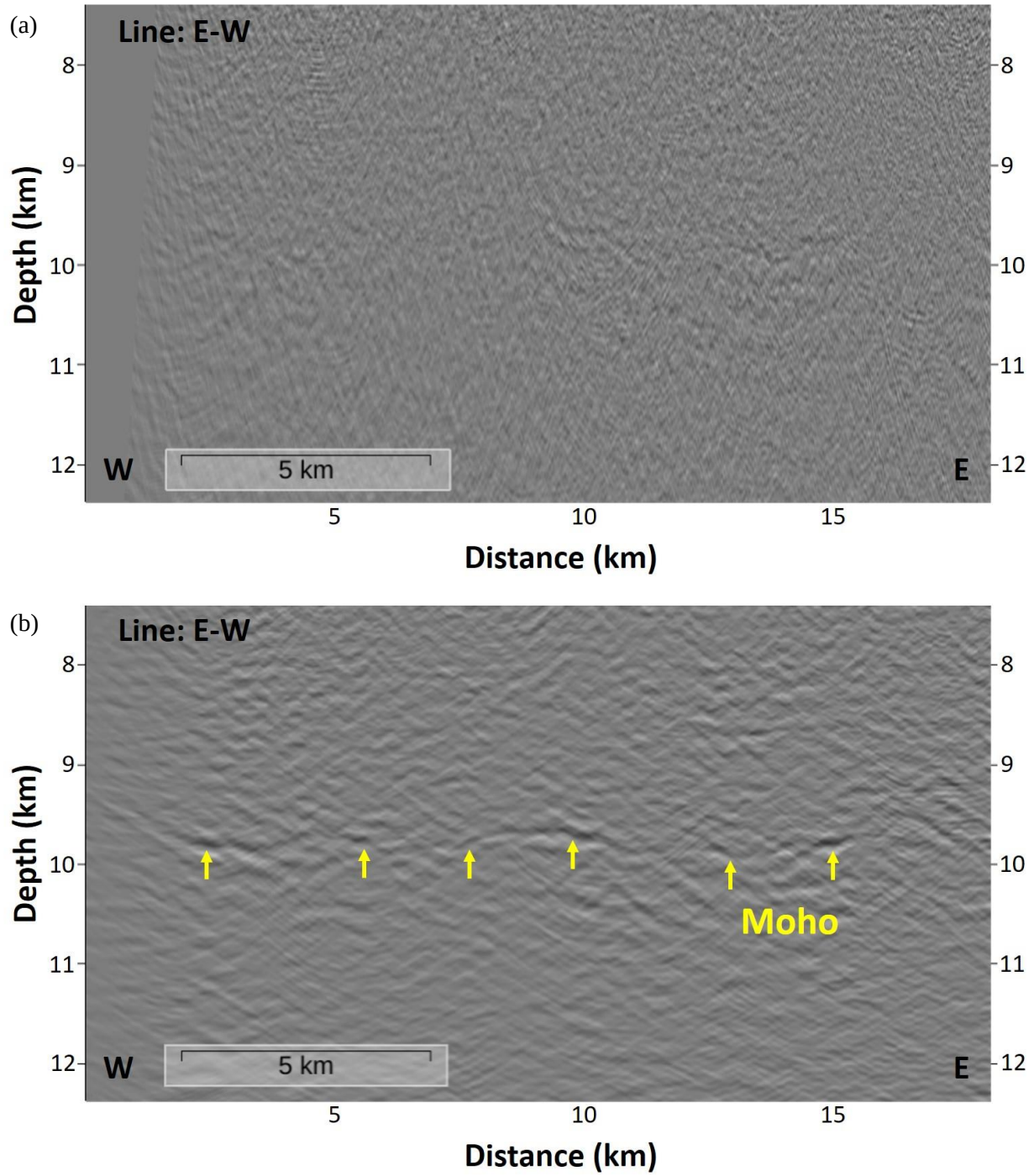

Figure 29 Post-SDM from previous study (Ohira et al., 2018), (a), and PSDM from our processing, (b), in the western section of Line E-W (Fig. 18a). Flat Moho reflection response is located at 9.5 km BSL in Line E-W. The Moho is not distinct in (a) but stronger in (b).

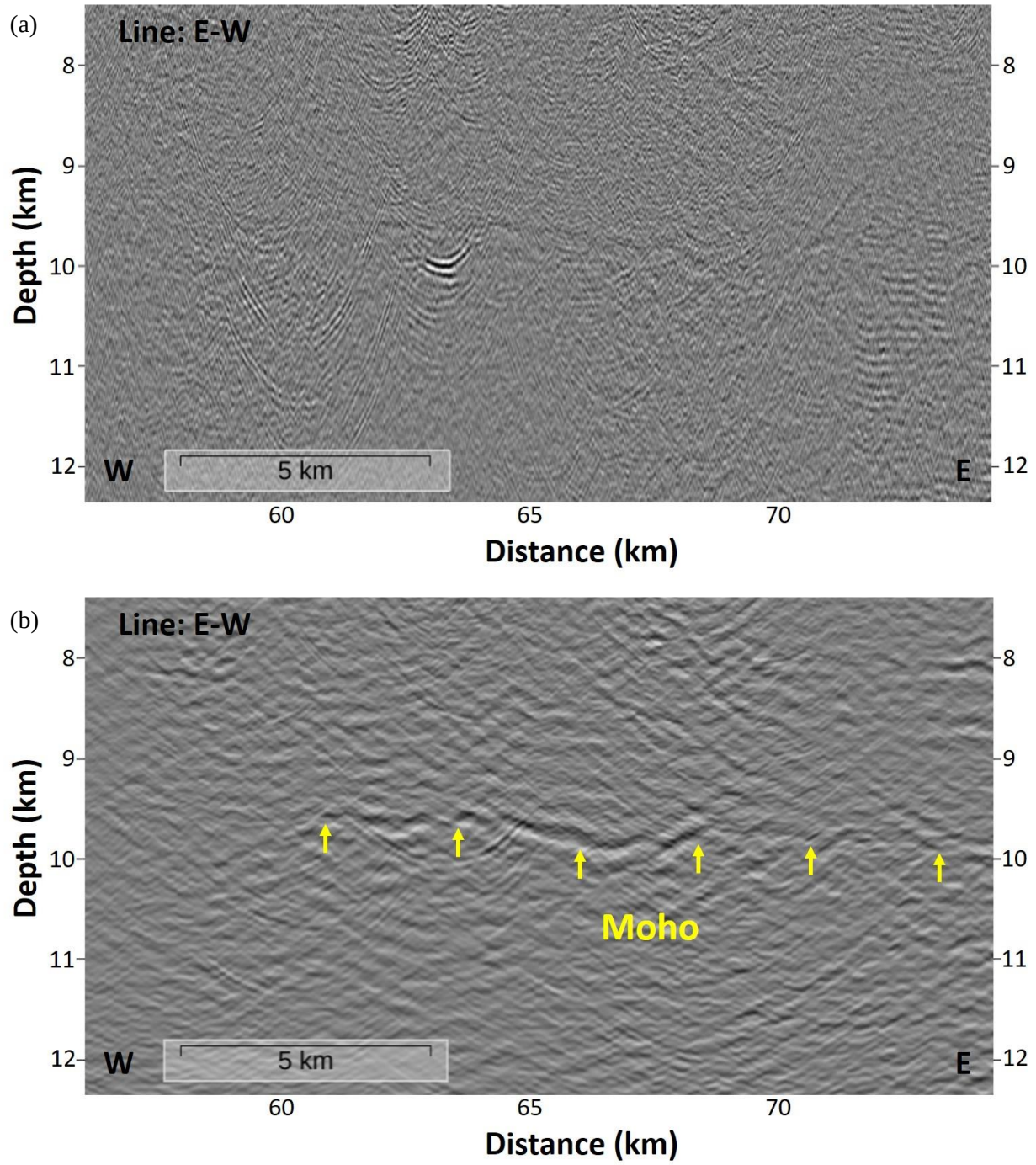

Figure 30 Post-SDM from previous study (Ohira et al., 2018), (a), and PSDM from our processing, (b), at 55 km from the western edge of Line E-W. The curved Moho is located at 60 km from western edge of the profile (Fig. 18a). The amplitude of Moho reflection is weak in the western section of this image, then become stronger for 8 km at the center of the image.

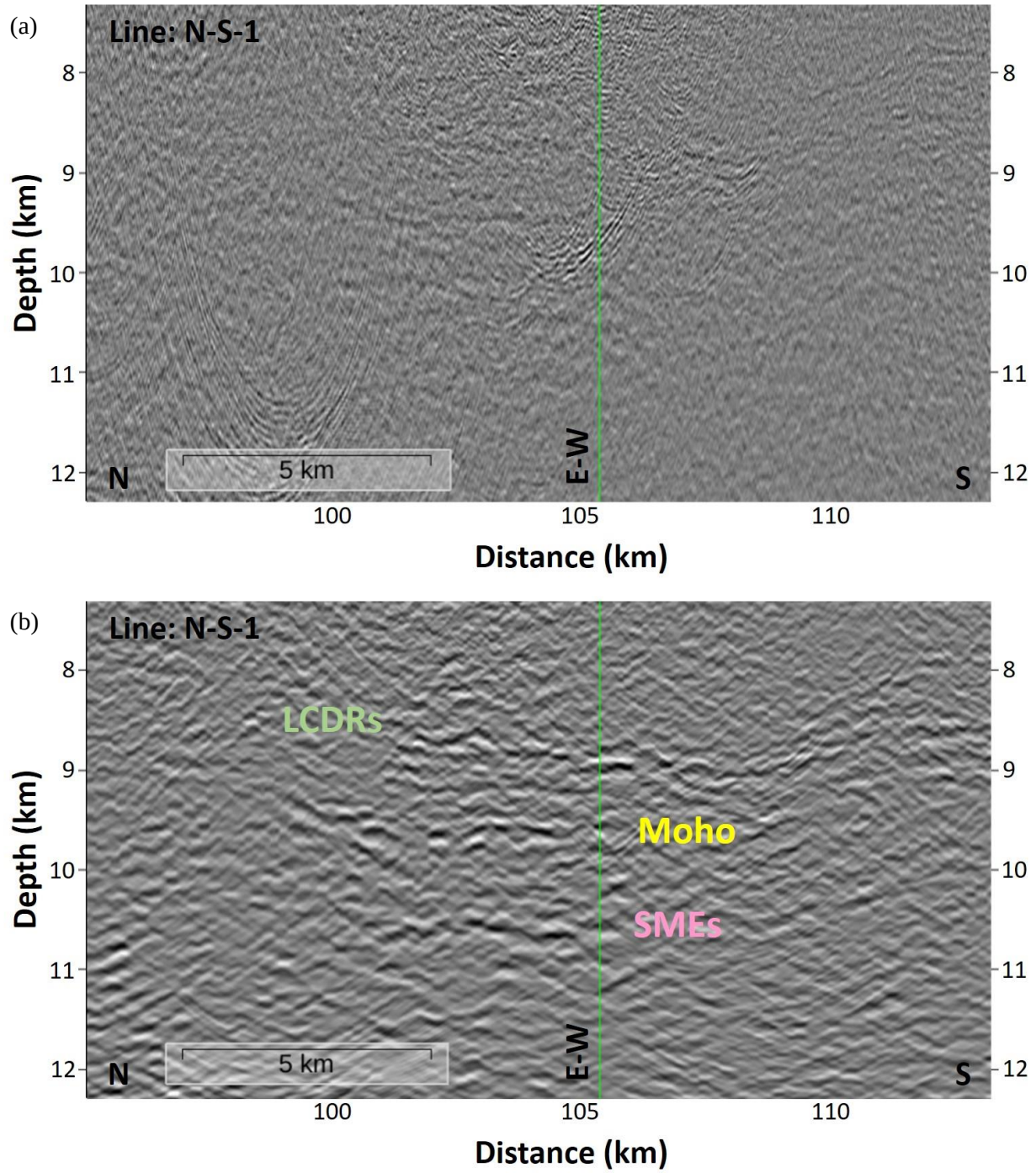

Figure 31 Post-SDM from previous study (Ohira et al., 2018), (a), and PSDM from our processing, (b), at the center of Line N-S-1 (Fig. 18b). Three main curved reflections from top to bottom illustrate LCDR, Moho and SME, respectively.

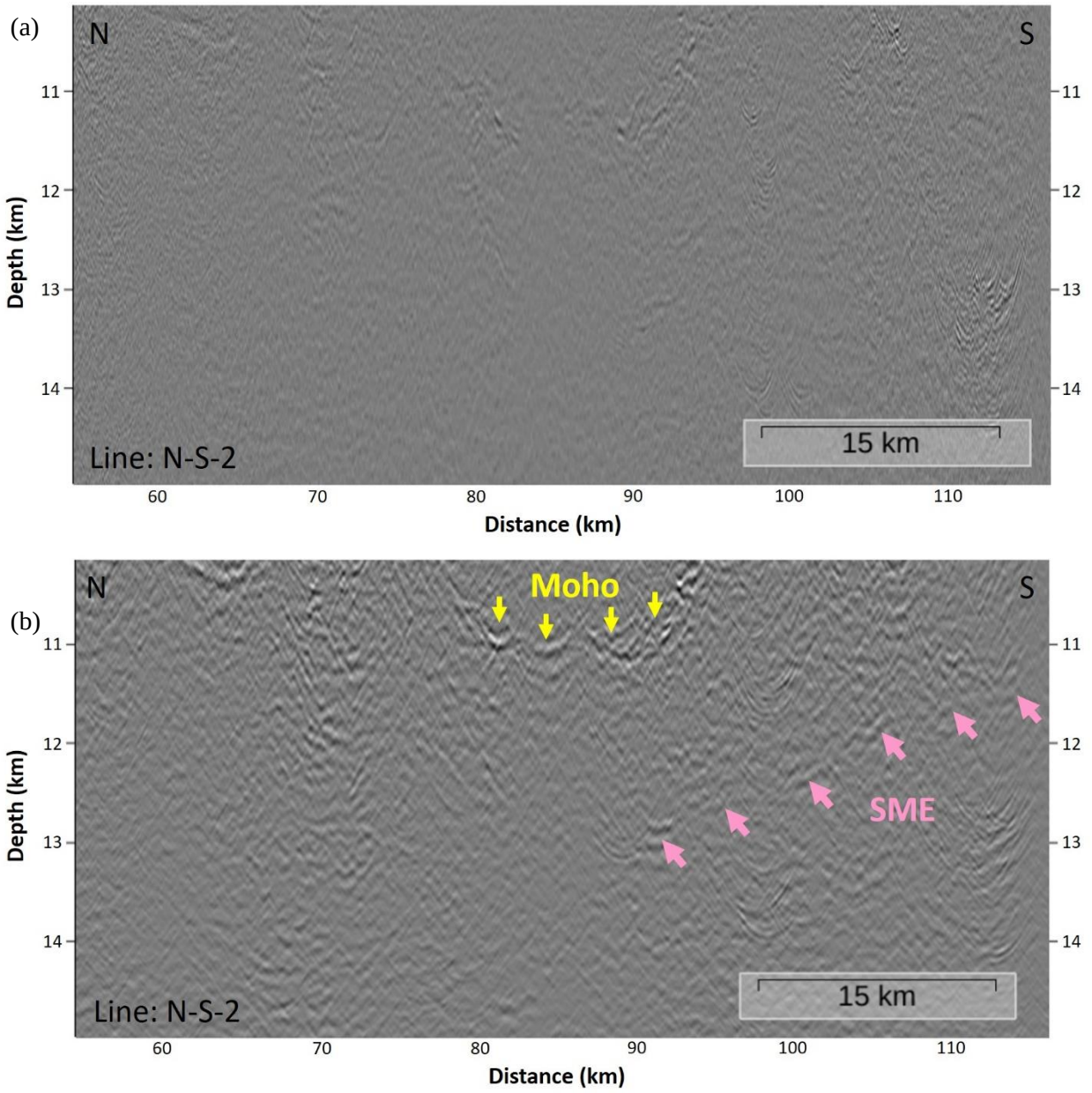

Figure 32 Post-SDM from previous study (Ohira et al., 2018), (a), and PSDM from our interpretation, (b), in the southern section of Line N-S-2 (Fig. 18c). Moho reflection response is indicated by the yellow arrows. SME is indicated by the pink arrows. A 30-km SME dips down northward by 5 degrees.

6. Conclusions

The Moho reflection and the oceanic crustal structure from 2-D MCS data, conducted along the NE Hawaiian Arch, were discussed in our study and compared with a previous study (Ohira et al., 2018). These seismic images illustrate the structures of the oceanic crust, especially in the lower crust, Moho, and below. The important features are summarized below:

1. The ~11-km LCDRs found in the eastern section of Line E-W may have originated from a secondary shear zone due to active magma upwelling. The LCDRs dip 5 to 12 degrees eastward, toward the paleo-ridge axis. Most of them terminate downward at the Moho.

2. The Moho reflections can be identified within ~50% of all lines, including the shingled Moho (5%) and a combination of the diffusive and weak Moho (45%).

3. The average thickness of oceanic crust is 5.4 km with a standard deviation of 0.3 km.

4. The MTZ is typically one km thick. The thick MTZs (>100m), imaged as the diffusive Moho, commonly accompany with SMEs.

Supplementary Information

(a)

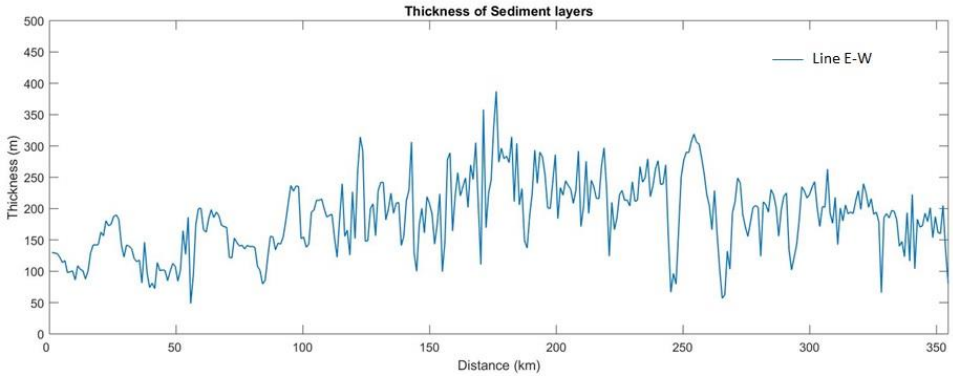

(b)

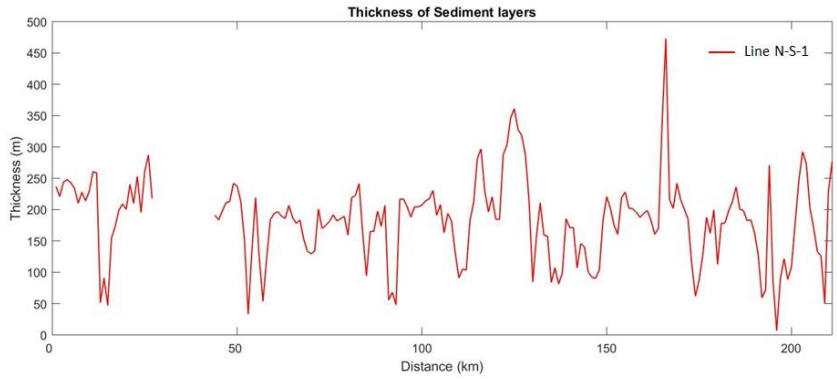

(c)

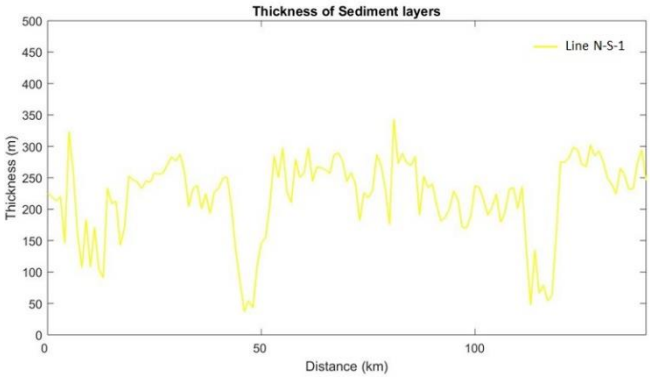

Figure I Thickness of sediment layers above the NE Hawaiian Arch with distance. (a), (b) and (c) are the crustal thickness of Line E-W, Line N-S-1 and Line N-S-2, respectively. The sediment is thinner at the seamounts. Thickness of sediment layers slightly fluctuates in Lines N-S and show linear trends. The trend of sediment thickness is not related to the seafloor depth.

(a)

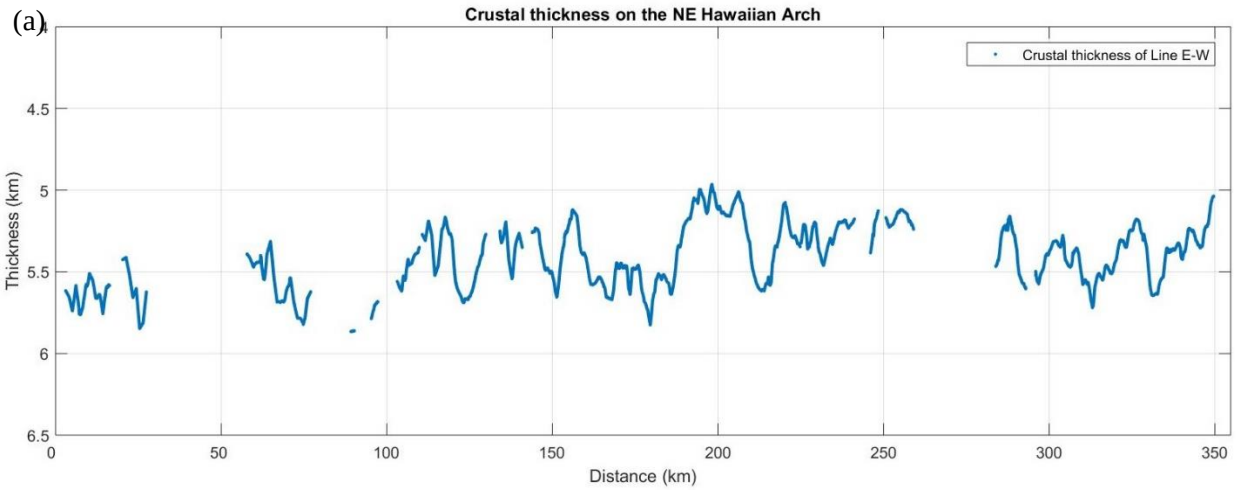

(b)

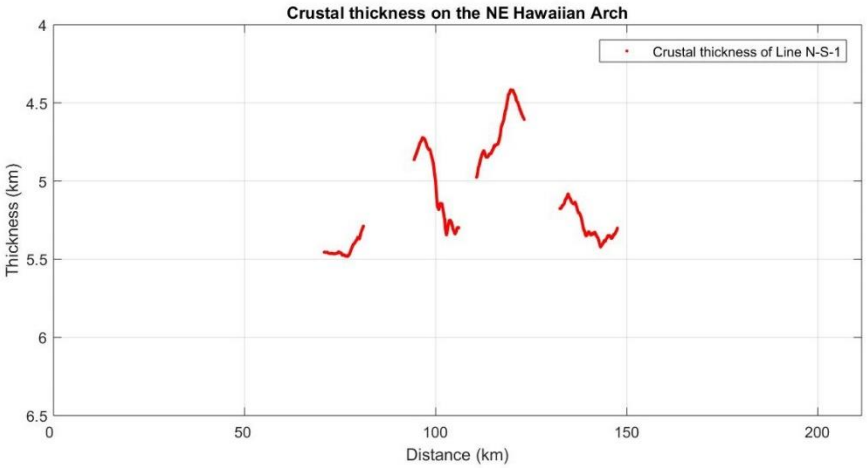

(c)

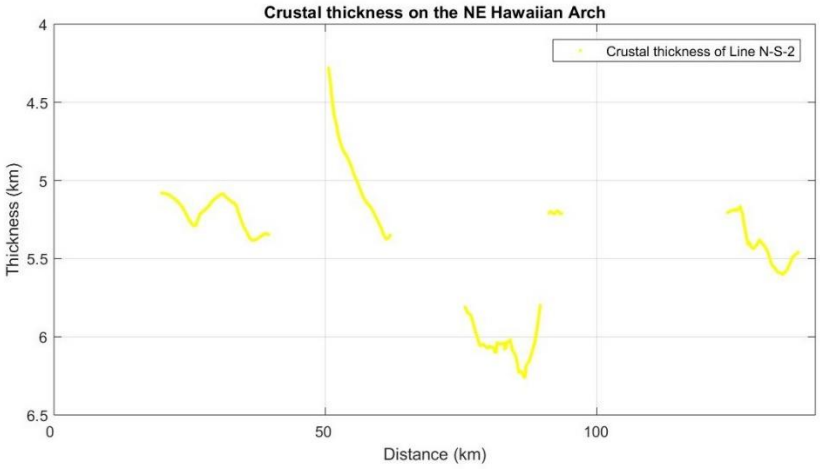

Figure II The oceanic crustal thickness with distance of all lines. (a), (b) and (c) are the crustal thickness of Line E-W, Line N-S-1 and Line N-S-2, respectively. The blue, red and the yellow dots indicate the thickness of oceanic crust in Lines E-W, N-S-1 and N-S-2, respectively.

Abbreviations

AFR	African plate
BSF	Below the seafloor
BSL	Below sea level
CDP	common depth point
DA	Degree of anisotropy
DSDP	Deep Sea Drilling Program
ESP	Expanding spread profile
FAR	Farallon plate
GRN	Greenland plate
IBR	Iberian plate
IODP	Integrated Ocean Drilling Program
IZA	Izanagi Ocean plate
JAMSTEC	The Japan Agency for Marine-Earth Science and Technology
JUN	Junction plate
LCDR	Lower crustal dipping reflection
LHR	Lord Howe Rise plate
MBSL	meter below sea level

MCS	Multi-channel seismic reflection
Moho	Mohorovičić discontinuity
MTZ	Moho transition zone
NMO	Normal moveout
ODP	Ocean Drilling Program
OBS	Ocean bottom seismometer
PAC	Pacific plate
PFR	Pacific-Farallon Ridge
Post-STM	Post-stack time migration
PSDM	Pre-stack depth migration
PSTM	Pre-stack time migration
SAM	South American plate
SME	Sub-Moho event
UCDR	Upper crustal dipping reflection
UCR	Upper crustal reflection
V_p	P-wave velocity

References

Aghaei, O., Nedimovic, M. R., Carton H., Carbotte, S. M., Canales, J. P., and Mutter, J. C. (2014). **Crustal thickness and Moho character of the fast-spreading East Pacific Rise from 9º42'N to 9º57'N from poststack-migrated 3-D MCS data**. *Geochem. Geophys. Geosyst., 15*, pp. 634–657. doi:10.1002/2013GC005069.

Bécel, A., Shillington, D. J., Nedimović, M. R., Webb, S. C., and Kuehn, H. (2015). **Origin of dipping structures in fast-spreading oceanic lower crust offshore Alaska imaged by multichannel seismic data.** *Earth Planet. Sci. Lett., 424*, pp. 26-37. https://doi.org/10.1016/j.epsl.2015.05.016.

Bianco, T. A., Garrett, I., Becker, J. M., and Garcia, M. O. (2005). **Secondary Hawaiian volcanism formed by flexural arch decompression**. *Geochem. Geophys. Geosyst.,* 6(8). https://doi.org/10.1029/2005GC000945.

Clague, D.A., and Dalrymple, G.B., 1989. **Tectonics, geochronology, and origin of the Hawaiian - Emperor volcanic chain.** *Geological Society of America, Geology of North America, N(12).*

Clague, D. A., Uto, K., Satake, K., and Davis, A. S. (2002). **Eruption style and flow emplacement in the submarine North Arch Volcanic Field, Hawaii, in Hawaiian Volcanoes: Deep Underwater Perspective**. *Geophys. Monogr. Ser., 128*, edited by E. Takahashi et al., pp. 65-84.

Conrad, C. P., Behn, M. D., and Silver, P. G. (2007). **Global mantle flow and the development of seismic anisotropy: Differences between the oceanic and continental upper mantle**. *J. Geophys. Res., 112*. doi:10.1029/2006JB004608.

Davis, A.S. and Clague, D.A. (2006). **Volcaniclastic deposits from the North Arch volcanic field, Hawaii: explosive fragmentation of alkalic lava at abyssal depths.** *Bull Volcanol, 68*, pp. 294-307. https://doi.org/10.1007/s00445-005-0008-7.

Dixon, J., Clague, D., Wallace, P., & Poreda, R. (1997). **Volatiles in Alkalic Basalts form the North Arch Volcanic Field, Hawaii: Extensive Degassing of Deep Submarine-erupted Alkalic Series Lavas**. *Journal of Petrology, 38(7)*, pp. 911-939.

Egbai, J. C., Atakpo, E. and Aigbogun, C. O. (2012). **Predictive deconvolution in seismic data processing in Atala prospect of rivers State, Nigeria.** *Pelagia Research Library, Advances in Applied Science Research, 3 (1)*, pp. 520-529. http://www.imedpub.com/articles/predictive-deconvolution-in-seismic-data-processing-in-atala-prospect-of-riversstate-nigeria.pdf

Fan, P. F., Grunwald, R. R. (1971). **Sediment distribution in the Hawaiian archipelago.** *Pacific Sci. 25(4)*, pp. 484-488.

Frey, F. A., Clague, D. A., Mahoney, J. J., Sinton, J. M. (2000). **Volcanism at the Edge of the Hawaiian Plume: Petrogenesis of Submarine Alkalic Lavas from the North Arch Volcanic Field**. *Journal of Petrology, 41(5)*, pp. 667-691. https://doi.org/10.1093/petrology/41.5.667.

Furumoto, A. S., Thompson, N. J., and Woollard, G. P. (1965). **The structure of Koolau volcano from seismic refraction studies.** *Pacific Sci., 19(3)*, pp. 306.

Furumoto, A. S. and Woollard, G. P. (1965). **Seismic Refraction Studies of the Crustal Structure of the Hawaiian Archipelago**. *Pacific Sci., 19(3)*, pp. 315-319.

Hallenborg, E., Harding, A., Kent, G., and Wilson, D. (2003). **Seismic structure of 15 Ma oceanic crust formed at an ultrafast spreading East Pacific Rise: Evidence for kilometer-scale fracturing from dipping reflectors**. *J. Geophys. Res.: Solid Earth, 108(B11).* https://doi.org/10.1029/2003JB002400.

Handschumacher, D. W. (2013). **Post-Eocene Plate Tectonics of the Eastern Pacific**. *Geophysical Monograph Series, the Geophysics of the Pacific Ocean Basin and Its Margin (eds G. H. Sutton, M. H. Manghnani, R. Moberly and E. U. Mcafee), 19(16).* doi:10.1029/GM019p0177.

Jacqueline, D. E., Clague, D. A., Wallace, P., Poreda, R. (1997). **Volatiles in Alkalic Basalts form the North Arch Volcanic Field, Hawaii: Extensive Degassing of Deep Submarine-erupted Alkalic Series Lavas**. *Journal of Petrology, 38(7),* pp. 911-939, https://doi.org/10.1093/petroj/38.7.911.

Jarchow, C. M., Thompson, G. A. (1989). **The Nature of the Mohorovicic Discontinuity**. *Ann. Rev. Earth Planet. Sci.,17(1),* pp. 475 -506.

Jones, T., and Nur, A. (1984). **The nature of seismic reflections from deep crustal fault zones**. *J. Geophys. Res., 89*, pp. 3153-3171.

Jousselin, D. and Nicolas, A. (2000). **The Moho transition zone in the Oman ophiolite-relation with wehrlites in the crust and dunites in the mantle**. *Marine Geophysical Researches, 21(3),* pp. 229-241.

Kent, G. M., Harding, A. J., Orcutt, J. A., Detrick, R. S., Mutter, J. C., and Buhl, P. (1994). **Uniform accretion of oceanic crust south of the Garrett transform at 14º15'S on the East Pacific Rise**. *J. Geophys. Res., 99*, pp. 9097–9116. https://doi.org/10.1029/93JB02872.

Kodaira, S., Fujie, G., Yamashita, M., Sato, T., Takahashi, T., and Takahashi, N. (2014). **Seismological evidence of mantle flow driving plate motions at a palaeo-spreading centre**. *Nature Geoscience, 7(5),* pp. 371-375.

McKenzie, D., Jackson, J., and Priestley, K. (2005). **Thermal structure of oceanic and continental lithosphere**. *Earth Planet. Sci. Lett., 233(3–4),* pp. 337-349. doi:10.1016/j.epsl.2005.02.005.

Morgan, J.P., and Chen, Y.J. (1993). **The genesis of oceanic crust: Magma injection, hydrothermal circulation and crustal flow**. *J. Geophys.Res., 98*, pp.6283–6297.

Müller, R. D., Sdrolias, M., Gaina, C., and Roest, W. R. (2008). **Age, spreading rates, and spreading asymmetry of the world's ocean crust**. *Geochem. Geophys. Geosyst., 9(4)*. doi:10.1029/2007GC001743.

Nedimovic, M. R., Carbotte, S. M., Harding, A. J., Detrick, R. S., Canales, J. P., Diebold, J. B., Kent, G. M., Tischer, M., and Babcock, J. M. (2005). **Frozen magma lenses below the oceanic crust**. *Nature, 436*, pp.1149-1152. doi:10.1038/nature03944.

Nicolas, A. (1994). **Comment on 'The genesis of oceanic crust: Magma injection, hydrothermal circulation and crustal flow' by Jason Phipps Morgan and Y. John Chen**. *J. Geophys. Res., 99*, pp.12029–12030.

Ohira, A., Kodaira, S., Nakamura, Y., Fujie, G., Arai, R., and Miura, S. (2017). **Structural variation of the oceanic Moho in the Pacific plate revealed by active-source seismic data.** *Earth Planet. Sci. Lett., 476,* pp. 111-121. http://doi.org/10.1016/j.epsl.2017.08.004.

Ohira, A., Kodaira, S., Moore, G., Yamashita, M., Fujiwara, T., and Kaiho, Y. (2018). **Active-source seismic survey on the northeastern Hawaiian Arch: Insights into crustal structure and mantle reflectors.** *Earth, Planets and Space, 70*, pp. 121. https://doi.org/10.1186/s40623-018-0891-8.

Reston, T. J., Ranero, C. R., and Belykh, I. (1999)**. The structure of Cretaceous oceanic crust of the NW Pacific: Constraints on processes at fast spreading centers.** *J. Geoph. Res., 104(B1),* pp. 629-644. https://doi.org/10.1029/98JB02640.

Rosa, A. L. R. (2018). **The seismic signal and its meaning**. *SEG, 23*, pp. 529. https://doi. 10.1190/1.9781560803348.

Rowan, C.J., and Rowley, D.B. (2014). **Spreading behaviour of the Pacific-Farallon ridge system since 83 Ma**. *Geophys. J. Int.*, http://dx.doi.org/10.1093/gji/ggu056.

Seton, M., Müller, R.D., Zahirovic, S., Gaina, C., Torsvik, T., Shephard, G., Talsma, A., Gurnis, M., Turner, M., Maus, S., and Chandler, M. (2002). **Global continental and ocean basin reconstructions since 200 Ma**. *Earth-Science Reviews, 113*(3-4), pp. 212-270.

Shor, G. G., and Pollard, D. D. (1964). **Mohole site selection studies north of Maui**. *J. Geoph. Res., 69(8),* pp. 1627-1638.

Singh S. C., Kent, G. M., Collier, J. S., Harding, A. J., and Orcutt., J. A. (1998). **Melt to mush variations in crustal magma properties along the ridge crest at the southern East Pacific Rise**. *Nature, 394(6696),* pp. 874–878.

Steinhart, J. S. (1967). **Mohorovičić discontinuity**. *In International Dictionary of Geophysics*, ed. S. K. Runcorn, 2, pp. 991-94.

The MELT Seismic Team (1998). **Imaging the Deep Seismic Structure Beneath a Mid-Ocean Ridge: The MELT Experiment**. *Science, New Series, 280, 5367*, pp. 1215-1218. https://www.jstor.org/stable/2896059.

Van Avendonk, H. J. A., Davis, J. K., Harding, J. L., and Lawver, L. A. (2017). **Decrease in oceanic crustal thickness since the breakup of Pangaea.** *Nature Geoscience, 10(1)*, pp. 58-61.

Vuong, K. A., Zhang, J., Gibson, L. R., Sager, W., 2011. **Analysis of marine multi-channel seismic data using a 2D continuous wavelet transform.** *AGU Fall Meeting Abstracts*, S23A-2235.

Watts, A. B., ten Brink, U. S., Buhl, P., Brocher, T. M. (1985). **A multichannel seismic study of lithospheric flexure across the Hawaiian-Emperor seamount chain**. *Nature, 315*, pp. 105. https://doi.org/10.1038/315105a0.

Wu, W. J. (2001). **The Advantage and Significance of Prestack Migration.** *SEG Technical Program Expanded Abstracts, 20(1)*, pp. 1037-1040.

Yilmaz, Öz (2001). **Seismic Data Analysis: Processing, Inversion, and Interpretation of Seismic Data** (Investigations in Geophysics, No. 10). *SEG, 10*. https://doi.org/10.1190/1.9781560801580.